Understanding the catalase-like activity of a bio-inspired manganese(II) complex with a pentadentate NSNSN ligand framework. A computational insight into the mechanism.

Maria Letizia Merlini,[a] George J. P. Britovsek,[b] Marcel Swart,*[c,d] Paola Belanzoni*[e,f]

a) Laboratoire de Chimie et Biochimie Computationnelles, Institut des Sciences et Ingénierie Chimiques, École Polytechnique Fédérale de Lausanne (EPFL), Av. F.-A. Forel 2, CH-1015 Lausanne, Switzerland

b) Department of Chemistry, Imperial College London, Exhibition Road, London, United Kingdom

c) Institut de Química Computacional i Catàlisi (IQCC) and Departament de Química, Universitat de Girona, Campus Montilivi, Facultat de Ciències, 17071 Girona, Spain

d) Institució Catalana de Recerca i Estudis Avançats (ICREA), Pg. Lluís Companys 23, 08010 Barcelona, Spain

e) Dipartimento di Chimica, Biologia e Biotecnologie, Università degli Studi di Perugia, Via Elce di Sotto 8, I-06123, Perugia, Italy

f) Istituto di Scienze e Tecnologie Molecolari del CNR (CNR-ISTM), c/o Dipartimento di Chimica, Biologia e Biotecnologie, Università degli Studi di Perugia, via Elce di Sotto 8, I-06123, Perugia, Italy

Abstract

The mechanism of H_2O_2 dismutation catalyzed by the recently reported 2,6-bis[((2-pyridylmethyl)thio)methyl]pyridine-Mn(II) complex ($[MnS_2Py_3(OTf)_2]$) has been investigated by density functional theory using the S12g functional. The complex has been analyzed in terms of its coordination properties and the reaction of $[MnS_2Py_3]^{2+}$ in a distorted square pyramidal coordination geometry with two hydrogen peroxide molecules has been investigated in our calculations. The sextet, quartet and doublet potential energy profiles of the catalytic reaction have been explored. In the first dismutation process the rate-determining step (RDS) is found to be the asymmetric O-O bond cleavage, which occurs on the sextet potential energy profile. A subsequent spin crossover from sextet to quartet can take place generating a stable Mn(IV) dihydroxo intermediate. This could disfavor the ping-pong mechanism commonly considered to describe the

H_2O_2 dismutation reaction, where the binding of the first H_2O_2 substrate leads to the release of one H_2O product and the conversion of the catalyst into a Mn(IV) oxo complex. The formation of this stable intermediate, featuring a peculiar trigonal prismatic coordination geometry paves the way for an alternative reaction pathway for the second dismutation process, termed the dihydroxo mechanism, where two water molecules and dioxygen are easily and simultaneously formed. The competing channels have different spin states: the sextet reaction pathway corresponds to the ping-pong mechanism, whereas the quartet reaction follows preferably the dihydroxo mechanism. The doublet reaction path is energetically disfavored for both channels. For the ping-pong mechanism, the RDS in the second dismutation process is represented by the second hydrogen-abstraction from H_2O_2, with a calculated energy barrier very close to that of the RDS in the first dismutation reaction. Explicit solvent molecules, counterions and trace amounts of water are found to further support the preference for the asymmetric O-O bond breaking, by favoring the end-on coordination mode of H_2O_2 to the catalyst.

Keywords: *bio-inspired manganese catalyst*, *H_2O_2 dismutation reaction*, *multispin-state mechanism*, *spin-crossover reactivity*, *DFT calculations*

1.Introduction

Oxygen, though essential for aerobic metabolism, can be converted into toxic metabolites, such as the superoxide anion (O_2^-), hydroxyl radical ($OH^\cdot$), and hydrogen peroxide (H_2O_2), collectively known as reactive oxygen species (ROS). ROS production is associated with numerous pathological conditions including ischemic and inflammatory processes.[1)] These powerful oxidants can attack proteins, lipids, lipoproteins, nucleic acids and carbohydrates,[2)] thereby turning into lethal agents against cell structure and functioning. *In vivo* protection occurs *via* mechanisms to control the level of ROS, including the use of two key classes of metalloenzymes, the superoxide dismutases (SOD)

and catalases (CAT), which catalyze the dismutation processes of superoxide and hydrogen peroxide, respectively. Although the majority of CATs rely on the heme group for catalysis, an alternative class of manganese-dependent CATs (MnCATs) has been identified in three different bacteria.[3)] Crystallographic studies have revealed that these MnCATs contain a dinuclear Mn core with bridging carboxylate and oxide ligands.[4)] Several studies have been dedicated to develop novel synthetic MnCATs biomimetic complexes.[5] The first example of a dinuclear Mn(II) catalyst mimicking the natural enzyme function has been reported by Dismukes and coworkers.[6] More recently, catalase biomimetics include single-site Mn complexes, often showing both SOD and CAT activity, which can be used as artificial small molecule catalysts for ROS detoxification and are promising as therapeutics.[7] Indeed, some Mn(III)-porphyrin (for example AEOL10150), Mn(III)-salen (for example EUK-113) and seven-coordinated Mn(II)-macrocyclic polyamine complexes (for example M40403) have entered clinical tests.[8-12] Although Mn-polyamine complexes show very high SOD-mimetic activity,[13] certain Mn-porphyrin and Mn-salen complexes exhibit dual SOD and CAT activity.[14-17]Additional functions of manganese complexes are known such as oxidation,[18-20] reduction,[21] or sulfur-oxygenation.[22]

In a recent paper by Britovsek, Bonchio and coworkers,[23] the synthesis and characterization of a bio-inspired Mn(II) complex with a linear pentadentate ligand framework containing soft sulfur donors and an alternating NSNSN binding motif is described. This seven-coordinate Mn(II) complex, with two triflate counterions, $[MnS_2Py_3(OTf)_2]$ (S_2Py_3 = 2,6-bis[((2-pyridylmethyl)thio)methyl]pyridine), displays excellent dual CAT/SOD-like antioxidant activity both in acetonitrile and in aqueous solution, with high turnover efficiency, surpassing the Mn(II) analogues with hard nitrogen and oxygen donor ligands $[Mn(NMe)_2Py_3(OTf)_2]$ ($(NMe)_2Py_3$ = N-methyl-(aminomethyl)pyridine), $[Mn(NTs)_2Py_3(OTf)_2]$ ($(NTs)_2Py_3$ = N,N'-ditosyl-2,6-bis[(2-pyridylmethyl)amino)methyl]pyridine), and $[MnO_2Py_3(OTf)_2]$ (O_2Py_3 = 2,6-bis[((2-pyridylmethyl)oxy)methyl]pyridine).[23] The CAT-like activity of the $[MnS_2Py_3(OTf)_2]$ complex, which is stable in an aqueous environment, is also higher than that of salen-type complexes, which

decompose irreversibly in water after several minutes. The pH of the solution appears to have a major influence on the stability of the catalyst. A very active and remarkably stable catalyst performance is generated by the addition of base (NaOH, 1M, 10μL) as well as by addition of imidazole in aqueous solution using a borate buffer (pH 9). The different reactivity of $[MnS_2Py_3(OTf)_2]$ containing sulfur donors compared to related ligands with N or O donors is unclear at this stage. However, a special role of sulfur ligation in biological systems based on manganese and related metal complexes, in particular cytochrome P450, is well documented.[18-22,24,25] The ability of sulfur donors to stabilize high valent metal complexes, while being susceptible to oxidation themselves, is not fully understood but must require careful balancing of the electronic and steric requirements. Noteworthy in this context, the sulfur donors in a manganese complex with a pentadentate thio-ketone-containing SNNNS ligand were found to inhibit antioxidant activity.[26]

An understanding of the mechanism of the catalase reaction is a fundamental task for ligand rational design and tuning of single-site manganese-based catalytic complexes in order to achieve improved catalase activity. Currently, only few examples of theoretical investigations of the hydrogen peroxide dismutation reaction ($2H_2O_2 \rightarrow 2H_2O + O_2$) mechanism are available in the literature and, to our knowledge, only using Mn(III)-salen complexes as catalysts. Abashkin and coworkers[27-29] presented the first theoretical investigations on Mn(III)-salen complexes (in particular, the EUK-8 complex) using density functional theory (DFT) in three different spin states singlet, triplet and quintet. The authors proposed the general ping-pong mechanism in which the first hydrogen peroxide molecule binds to the Mn(III) center, oxidizes the metal, and releases a water molecule while forming the oxomanganese intermediate Mn(V)=O. A second hydrogen peroxide molecule reacts with the oxomanganese species and the oxygen atom is transferred to hydrogen peroxide forming dioxygen and water. The experimental study reported by Nocera and coworkers[30] concurred with the DFT prediction by Abashkin.

Theoretical studies on the mechanism of functional biomimetics of enzymes, although fundamentally important for a better understanding of the enzyme and the design of MnCATs with

improved therapeutic properties, is a challenging task: different spin states are usually involved but many standard DFT functionals fail to predict the correct energy relationship between them.[31,32] For our investigations we used the S12g functional which has been recently recognized as a reliable tool for providing a correct picture of the spin state energy order in complicated transition metal systems and its accurate performance is well documented.[33-35]

We are not aware of any studies in the literature on the mechanism of catalase-type reactions catalyzed by the pentadentate NSNSN-Mn(II) complex. This is precisely the aim of this work. We present here our S12g DFT investigation on the mechanism of H_2O_2 dismutation reaction catalyzed by the [Mn(II)$S_2Py_3(OTf)_2$] complex on the three different potential energy surfaces of the doublet, quartet and sextet spin states.

2. Methods and Computational Details

A comprehensive DFT computational study was performed using the ADF2014.05[36-38] and the related Quantum-regions Interconnected by Local Descriptions (QUILD) program[39)] to identify the structures of the reactant complexes, intermediates, transition states and product complexes of the hydrogen peroxide dismutation reaction catalyzed by $[MnS_2Py_3]^{2+}$. For geometry optimizations, calculations were carried out using the GGA functional BP86,[40,41] including Grimme's D_3 dispersion correction (BP86-D_3).[42] All atoms were described with a Slater-type DZP double-ζ quality basis set (TZP triple-ζ for Mn), using the frozen core approximation (core small). Solvation effects have been taken into account by the Conductor like Screening Model COSMO[43-45] using acetonitrile as solvent and the default COSMO surface in ADF2014.05 version (Esurf). Relativistic effects were treated with the scalar zero-order regular approximation, ZORA model.[46,47] Final energies have been calculated by single point S12g functional[33)] calculations on the optimized BP86-D_3/DZP solution phase structures with a TZ2P triple-ζ quality basis set with two polarization functions (core small) for all atoms. As mentioned above, the S12g functional has been shown to be

a reliable tool for the energetics of spin states and to improve significantly the prediction of the reaction barriers in transition metal systems.[34,48] This spin-state consistent S12g density functional was designed to work well for spin states based on the observation[49] that the difference between the good (OPBE) and bad (PBE) performance for spin states[50] can be traced back to the region of s<1 in the exchange enhancement factor. This was used to design the SSB-D[51] and S12g[33] functionals, including Grimme dispersion.[52,53] Frequency calculations at the same S12g/TZ2P level of theory have been also performed to identify all stationary points as minima (zero imaginary frequencies) or transition states (one imaginary frequency) and to compute the Gibbs free energies. For all calculations carried out with BP86-D_3 the Becke grid of Normal quality was employed, whereas S12g calculations were performed with a Becke grid of VeryGood quality.[54] All DFT calculations were carried out using the unrestricted Kohn-Sham scheme for the open shell sextet, quartet and doublet spin states.

3. Results and Discussion

The initial complex

To avoid uncertainties connected with using an incomplete model,[29] the entire complex reacting with hydrogen peroxide will be considered in our DFT calculations. To this aim, since no X-ray crystal structure of $[MnS_2Py_3(OTf)_2]$ is available yet, preliminary geometry optimizations to analyze the coordination behavior of seven- and five-coordinate Mn(II) complexes have been performed for the experimentally measured sextet spin state. The ^{19}F NMR spectrum for $[MnS_2Py_3(OTf)_2]$ in CD_3CN at room temperature (see Fig. S4 ESI in ref [23]) supports a six-coordinate geometry, with the NSNSN ligand in a *fmf* coordination mode (for octahedral complexes the ligand coordination mode is conveniently described using the meridional (*m*) and facial (*f*) notation for each consecutive set of three donors within the ligand, *fmf* = fac-mer-fac), with one

triflate ligand occupying the axial position and the other in the second coordination sphere. Triflate ligands are generally weakly coordinating and are easily displaced in acetonitrile or aqueous solution. For example, a dynamic equilibrium between two iron(II) complexes with the related pentadentate ligand 2,6-bis[(methyl(2-pyridylmethyl)amino)-N-methyl]pyridine and two triflate anions, one with a seven-coordinate pentagonal bipyramidal geometry and the other with a five-coordinate trigonal bipyramidal geometry upon loss of the two triflate ligands, has been previously reported.[55] Moreover, based on the XRD structure of the oxygen-containing analogue $[MnO_2Py_3(OTf)_2]$,[23] which shows a distorted pentagonal bipyramidal coordination geometry with two triflate ligands in the axial positions, a possible 7-5 coordination equilibrium could have an important impact on the study of $[MnS_2Py_3(OTf)_2]$ in solution, where spin and coordination equilibria are essential features of its catalytic action. To ascertain the geometrical structure, a detailed study of the $[MnS_2Py_3(OTf)_2]$ complex in the sextet (S = 5/2) spin state, through COSMO solvent calculations, also including two explicit solvent molecules in the second coordination sphere, is reported in the SI (Figures S1-S4). The most stable species is shown in Figure 1 (left), where the ligand has a *fmf* coordination mode, with one triflate ligand in the axial position, in agreement with the octahedral geometry supported by NMR spectroscopy.

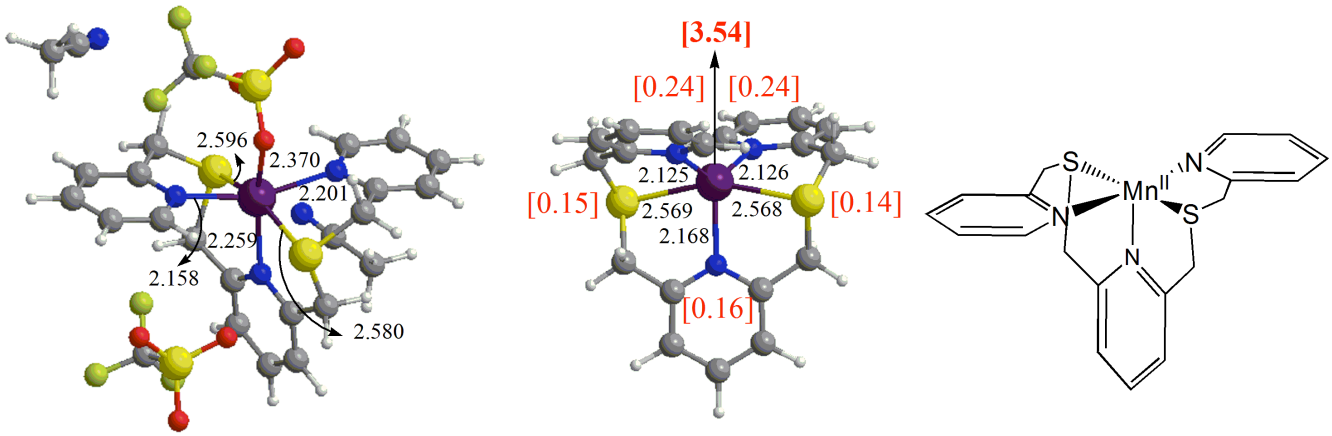

Figure 1. Left) Optimized geometry of the most stable coordination geometry (denoted SBPY-6 [OTf] in Figure S1 in the SI) of the $[MnS_2Py_3(OTf)_2]$ complex (two explicit acetonitrile solvent molecules are also included) in the sextet (S=5/2) spin state. Middle) Optimized geometry of the most stable $[MnS_2Py_3]^{2+}$ complex in the sextet spin state. Right) Schematic picture of the initial catalyst $[MnS_2Py_3]^{2+}$ complex under investigation. Distances are in Å. Values in square bracket refer to the calculated spin densities (based on Multiple Derived Charges (MDC-q) analysis[56]) on Mn and N,S donor atoms.

A similar COSMO solvent analysis has been carried out on the bare $[MnS_2Py_3]^{2+}$ complex, in the absence of triflate ions and explicit solvent molecules, showing that the sextet spin state (S=5/2) is the ground state, with the quartet (S=3/2) and the doublet (S=1/2) spin states lying at higher energies in the order. We have found that the most stable geometry for the $[MnS_2Py_3]^{2+}$ complex can be described as distorted square pyramidal with the two nitrogen donors of the terminal Py rings and the two sulfur atoms in the equatorial plane and the nitrogen atom of the central Py ring representing the apical position of the pyramid (see Figure 1 middle). This geometry is also seen in related Group 12 metal complexes of zinc and mercury with this ligand.[57] Due to the absence of any crystal field stabilization energy for d^{10} and HS d^5 metal complexes, the coordination

geometries are largely dictated by steric effects.

For our mechanistic study we therefore considered $[MnS_2Py_3]^{2+}$ with an open coordination site at the axial position of a pseudo octahedral geometry (see Figure 1 right) in a sextet spin ground state as the initial catalyst precursor complex, which is in agreement with both the experimental ^{19}F NMR spectrum and the experimental magnetic moment value of 5.9-6.0 μ_B (Fig. S4 and S1 ESI in ref. [23]). A description of the spin density distribution in the $[MnS_2Py_3]^{2+}$ initial complex (IC) is given in Figure 1 (middle). In the sextet spin state the spin density on Mn is 3.54, less than the expected 5 α-spin unpaired electrons for a high-spin d^5 Mn(II) metal atom. Interestingly, additional spin density delocalizes over the N (0.24, 0.16 and 0.24) and S donor atoms (0.14 and 0.15) of the ligand (total 0.93), which leads to an overall electronic structure in the sextet state (roughly 4 α-spin unpaired electrons on Mn and 1 α-spin unpaired electron on the ligand). According to our description, the manganese ion in the initial complex $[MnS_2Py_3]^{2+}$ should bear a physical oxidation state III. This finding suggests that the ligand can display non-innocent character. Redox non-innocence of S-containing ligands is not unprecedented and has been extensively illustrated by Wieghardt and Sproules[58] in their seminal work on transition metal bis(dithiolene) complexes by probing the sulfur composition of the frontier orbitals. The five singly occupied molecular orbitals for the initial $[MnS_2Py_3]^{2+}$ complex are presented in Figure 2, with their percentage compositions (main contributions in terms of individual N, S and Mn atoms) and energies.

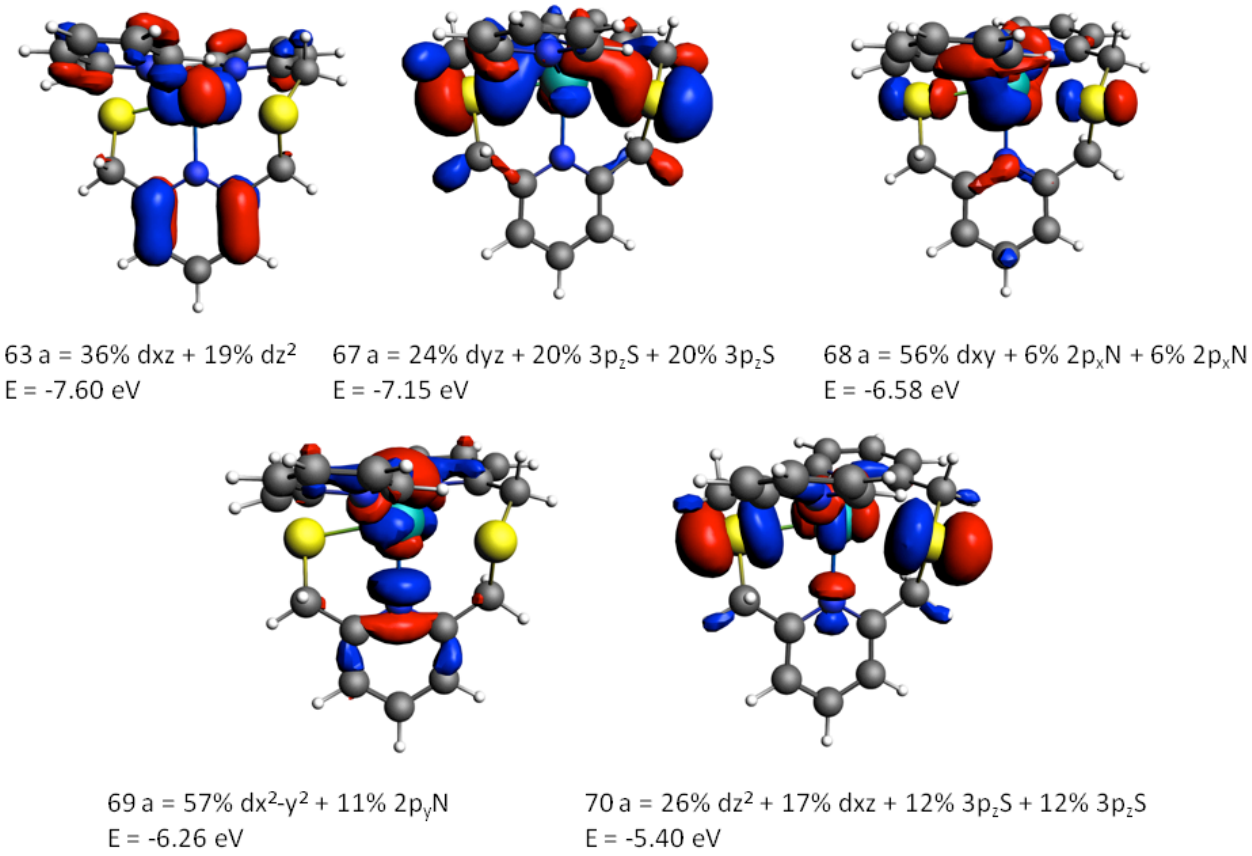

Figure 2. Singly occupied MOs (α spin), percentage compositions (main contributions of individual Mn, N and S atoms) and energies for the initial complex $[MnS_2Py_3]^{2+}$. The y axis is oriented along the Mn-N axial ligand, the z axis along the equatorial S-Mn-S and the x axis along the equatorial N-Mn-N direction.

The lower lying MO (63 a) in this set is mainly a Mn dxz/dz^2 hybrid orbital with no involvement of N and S donor atoms. A substantial S $3p_z$ character is observed in the 67 a (dyz) and 70 a (dz^2/dxz) MOs, whereas 68 a (dxy) MO has contributions from equatorial N $2p_x$ orbitals and 69 a (dx^2-y^2) MO from axial N $2p_y$ orbital, providing evidence of the non innocent nature of the NSNSN ligand which, interacting with the five d metal orbitals, acquires a total of 1 unpaired electron delocalized over the N/S donor atoms.

First dismutation reaction

In this subsection, we investigate the first dismutation reaction of one hydrogen peroxide molecule catalyzed by the $[MnS_2Py_3]^{2+}$ complex, which can take place for three different spin states of Mn(II) (sextet, quartet and doublet). According to the ping-pong mechanism commonly reported in the literature,[27-29] the first dismutation reaction leads to the simultaneous formation of a water molecule and an oxo manganese intermediate. The coordination of hydrogen peroxide to the Mn(II) metal (denoted RC_I in Scheme 1), which induces the O-O bond cleavage, could in principle provide a high-valent manganese (IV) oxo compound (PC_{Ioxo}) through the formation of a monohydroxo (plus free hydroxide) (I_{OH}) or via a stable dihydroxo intermediate (I_{OHOH}) (see Scheme 1). As recognized by several reports, [59-65] manganese(IV) dihydroxo intermediates are potentially capable of hydrogen abstraction and therefore could represent key active intermediates and alternatives to manganese(IV) oxo compounds for the subsequent second dismutation reaction.

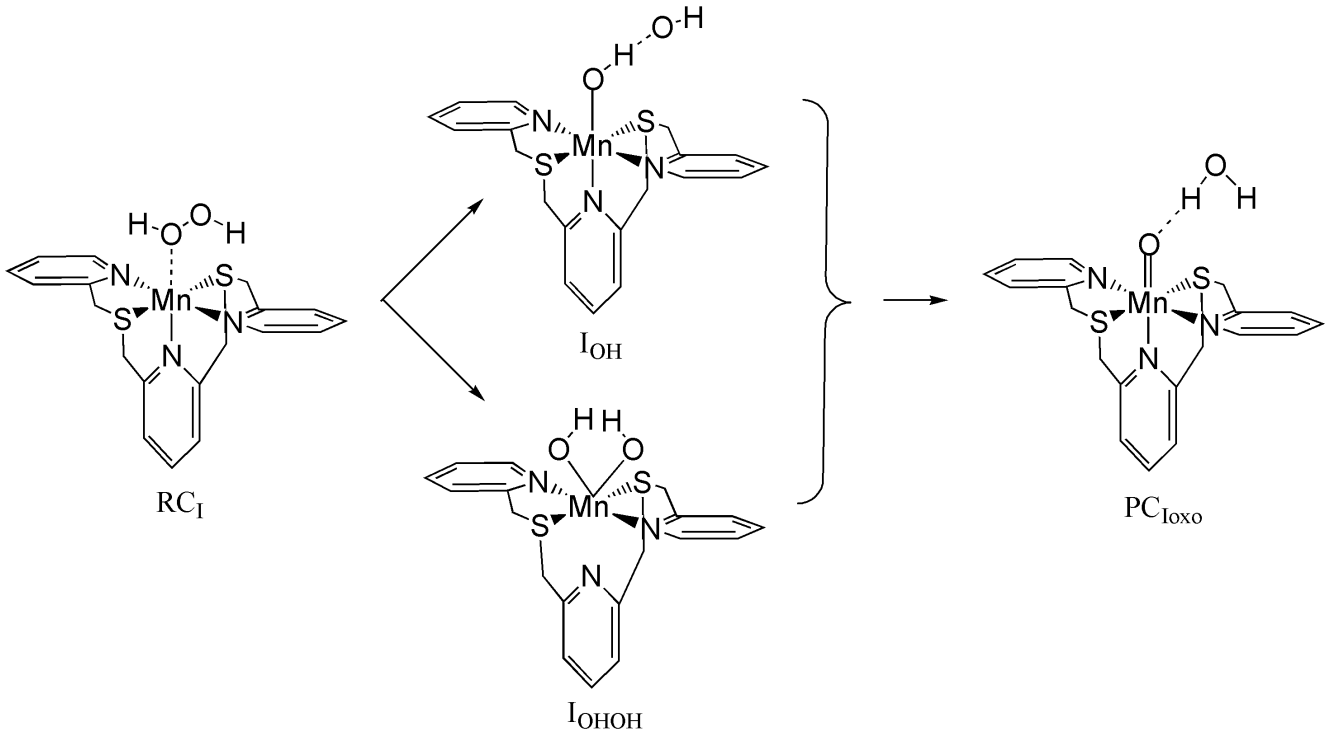

Scheme 1. Proposed intermediates and products of the first dismutation reaction of hydrogen peroxide catalyzed by $[MnS_2Py_3]^{2+}$: RC_I represents the reactant complex, I_{OH} the Mn monohydroxo intermediate, I_{OHOH} the Mn(IV) dihydroxo intermediate and PC_{Ioxo} the Mn(IV) oxo intermediate plus a product water molecule.

The question we address here is whether the first dimutation reaction with $[MnS_2Py_3]^{2+}$ can be described with the classical ping-pong mechanism leading to the formation of an oxo manganese(IV) intermediate and a water molecule (PC_{Ioxo}) or with a different mechanism, involving the formation of a stable dihydroxo Mn(IV) intermediate (I_{OHOH}).

The reactant complex

The optimized geometries of the reactant complexes, denoted RCx (x=s for sextet, x=q for quartet and x=d for doublet), in the three different spin states are shown in Figure 3.

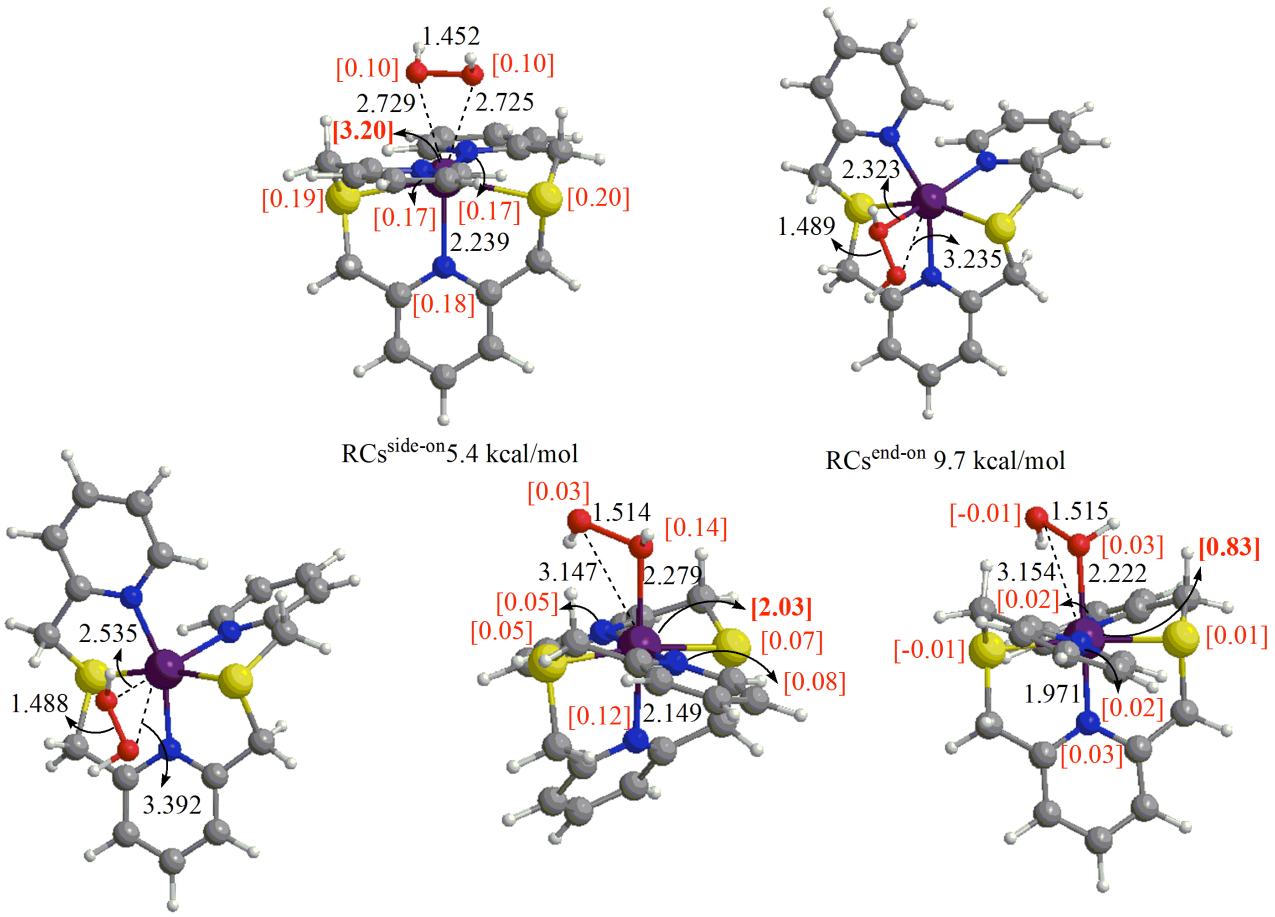

Figure 3. Optimized geometries of the reactant complexes $[MnS_2Py_3(H_2O_2)]^{2+}$ in the sextet ($RCs^{side\text{-}on}$, $RCs^{end\text{-}on}$), quartet ($RCq^{end\text{-}on}$, $RC'q^{end\text{-}on}$) and doublet ($RCd^{end\text{-}on}$) spin states. Distances are in Å and Gibbs free energies are given in kcal/mol with respect to the sum of the Gibbs free energies of the separate reactants ($[MnS_2Py_3]^{2+}$ + H_2O_2) in their spin ground states taken as zero reference energy. Values in square brackets are spin densities (based on Multiple Derived Charges (MDC-q) analysis) calculated on Mn, N and S atoms.

For the sextet spin state the reactant complex has been calculated for two different coordination modes: one showing an end-on binding of the hydrogen peroxide molecule to the metal center (denoted $RCs^{end\text{-}on}$, Mn-O1 = 2.323 Å, Mn-O2=3.235 Å), the other a side-on approach of the substrate (denoted $RCs^{side\text{-}on}$ Mn-O1 = 2.725 Å, Mn-O2=2.729 Å). Additionally, the coordination mode of the pentadentate ligand changes from *mmf* in $RCs^{end\text{-}on}$ to *fmf* in $RCs^{side\text{-}on}$. The latter is more stable by 4.3 kcal/mol, but both $RCs^{side\text{-}on}$ and $RCs^{end\text{-}on}$ are less stable than the sum of the Gibbs free energies of the separate reactants ($[MnS_2Py_3]^{2+}$ + H_2O_2) by 5.4 and 9.7 kcal/mol, respectively. The binding of hydrogen peroxide is endothermic in the sextet spin state. The participation of similar species in catalytic processes has been invoked, for instance, for Mn-porphyrin complexes, and it was also suggested that the O-O bond of H_2O_2 coordinated in the side-on mode may dissociate, resulting in two OH groups bound to the metal center.[66] However, it should be noticed that, apart from the different approaches of H_2O_2 to Mn, coordination of H_2O_2 occurs in a cis position with respect to the central Py ring of the ligand in the $RCs^{end\text{-}on}$ structure, whereas in $RCs^{side\text{-}on}$ it takes place trans to it, thus retaining the initial catalyst coordination mode (see Figure 1 left). This finding suggests that the NSNSN ligand is flexible enough to cope with substrate coordination. The different coordination mode (ligand plus substrate) around the central

metal can also account for the less stable $RCs^{end\text{-}on}$ reactant complex. In the quartet spin state, two different structures have been calculated, both showing an end-on approach of H_2O_2 to Mn. They differ not only in the Mn-O distances, but also in the O-O bond lengths. In $RCq^{end\text{-}on}$ the hydrogen peroxide is positioned above the metal center at large distance (Mn-O1=2.535 Å, Mn-O2=3.392 Å), whereas in $RC'q^{end\text{-}on}$ one oxygen atom of H_2O_2 binds to Mn (Mn-O1=2.279 Å, Mn-O2=3.147 Å), leading to an increase of the O-O bond length from 1.488 Å in $RCq^{end\text{-}on}$ to 1.514 Å in $RC'q^{end\text{-}on}$ (Figure 3). In addition, in $RCq^{end\text{-}on}$ the NSNSN ligand binds in a *mmf* mode, with a terminal Py ring of the ligand occupying the axial position trans to the substrate, as found in the $RCs^{end\text{-}on}$ structure. Both $RCq^{end\text{-}on}$ and $RC'q^{end\text{-}on}$ are less stable than the sum of the Gibbs free energies of the separate reactants by 25.1 and 34.2 kcal/mol, respectively. Finally, in the doublet spin state, only one $RCd^{end\text{-}on}$ structure has been found with a *fmf* coordination mode and an end-on coordination of hydrogen peroxide to Mn (Mn-O1=2.222 Å, Mn-O2=3.154 Å), and an elongated O-O bond (O-O=1.515 Å), with a Gibbs free energy of 30.3 kcal/mol with respect to the sum of the Gibbs free energies of the separate reactants in their ground spin states.

It is of interest at this stage to describe the three possible spin multiplicities of the reactant complex (doublet, quartet and sextet) in terms of their spin density distribution. Values of spin densities calculated on Mn and the N and S donor atoms are presented in Figure 3 for $RCs^{side\text{-}on}$, $RC'q^{end\text{-}on}$ and $RCd^{end\text{-}on}$. The spin density distribution over the metal and the ligand in $RCs^{side\text{-}on}$ is very similar to that found in the initial complex (see Figure 2 middle)): the spin density delocalizes over the Mn (3.20), the N (0.17, 0.18, 0.17) and the S (0.19, 0.20) donor atoms, and, in addition, over the O atoms of the H_2O_2 substrate (0.10, 0.10), with approximately four unpaired electrons on Mn and one unpaired electron on the ligand and substrate. A less delocalized spin density distribution is found for the reactant complex in the quartet state $RC'q^{end\text{-}on}$ with spin densities on Mn (2.03), N (0.08, 0.12, 0.05) and S (0.05, 0.07) and on the H_2O_2 oxygen atom bound to the metal (0.14), roughly corresponding to three unpaired electrons on the Mn(II) center, and even less for the reactant complex in the doublet state $RCd^{end\text{-}on}$, with a spin density on Mn of 0.83, corresponding to one

unpaired electron on Mn(II). Involvement of ligand spin density decreases on moving from sextet to quartet and to doublet spin states.

Starting from the above $RCs^{side\text{-}on}$ reactant complex, the bond between the oxygen atoms of the hydrogen peroxide is broken and two possible scenarios can be hypothesized: one leading to a Mn(IV) dihydroxo species as the first dismutation reaction product, the other leading to a Mn(IV) oxo species, either via the formation of a dihydroxo or a monohydroxo intermediate (Scheme 1).

Symmetric vs. asymmetric O-O bond breaking: formation of the intermediate species

Firstly we analyzed the formation of the Mn dihydroxo species, which is expected to occur via a symmetric O-O bond cleavage. The energy profile is depicted in Figure 4, whereas the transition state and the intermediate structures in the sextet, quartet and doublet spin states with relevant geometrical parameters are reported in the SI (Figure S5).

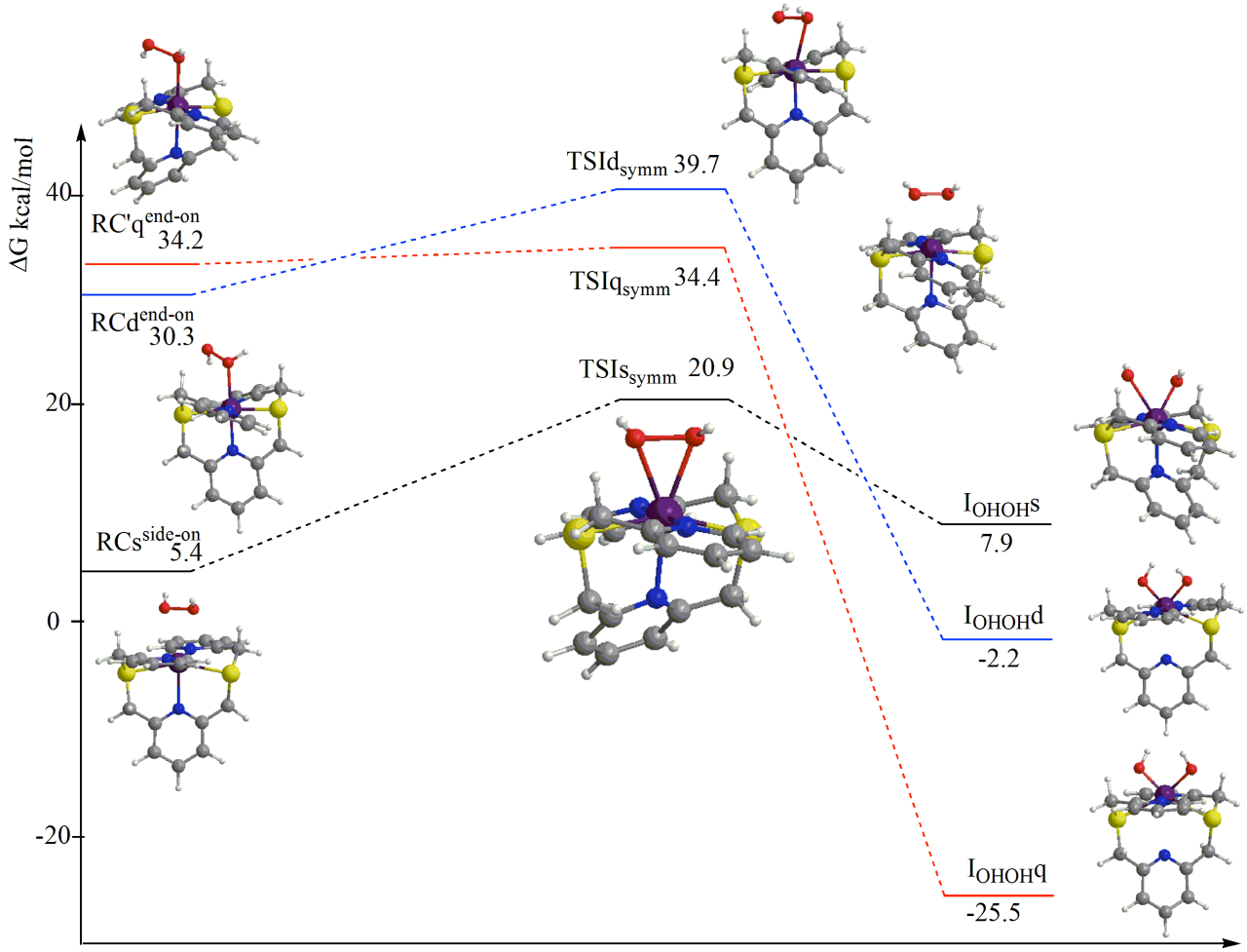

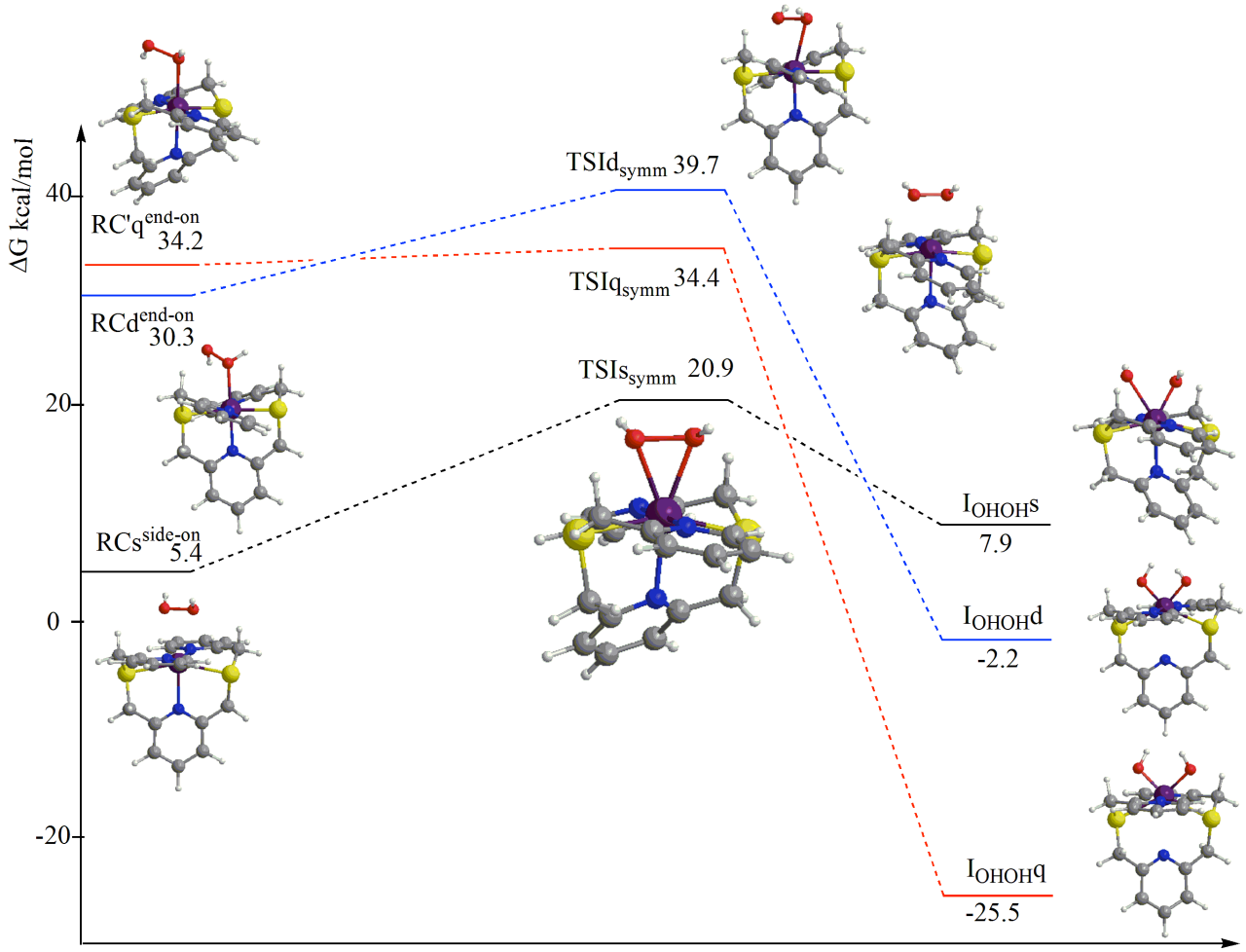

Figure 4. Energy profile of the manganese dihydroxo intermediate formation via a symmetric O-O bond breaking for sextet (black), quartet (red) and doublet (blue) spin states. The sum of the Gibbs free energies of the separate reactants ($[MnS_2Py_3]^{2+}$ + H_2O_2) is taken as the zero reference energy.

The energy profile shows that the sextet state is the lowest spin state for the reactant complexes (both $RCs^{side\text{-}on}$ and $RCs^{end\text{-}on}$) until the transition state $TSIs_{symm}$ is reached with an activation energy barrier of 15.5 kcal/mol (20.9 kcal/mol above the isolated reactants). The most stable O-O bond breaking process product, the dihydroxo species $I_{OHOH}x$ (x=s,q,d), is in the quartet spin state. A spin transition from the sextet to the quartet state occurs going to the dihydroxo complex $I_{OHOH}q$. The doublet spin state profile also crosses the sextet spin state after the transition state but the corresponding dihydroxo species $I_{OHOH}d$ is less stable than $I_{OHOH}q$ by 23.3 kcal/mol. The formation

of $I_{OHOH}q$ is exothermic by 25.5 kcal/mol with respect to the separate reactants.

The $TSIs_{symm}$ essentially describes the symmetric breaking of the O-O bond, with an elongated O-O distance of 1.695 Å compared to 1.452 Å in the $RCs^{side\text{-}on}$ complex, and with similar Mn-O distances (Mn-O1 = 2.293 Å and Mn-O2=2.286 Å). In $TSIq_{symm}$ and $TSId_{symm}$ the O-O distance is shorter (1.487 Å and 1.488 Å, respectively) than in $TSIs_{symm}$ (1.695 Å). In the $I_{OHOH}q$ structure two symmetric metal-hydroxo bonds are formed (Mn-O1 = Mn-O2 = 1.830 Å) at the expense of the Mn-N pyridine bond trans to the two hydroxo ligands which elongates significantly (Mn-N = 2.917 Å vs. Mn-N=2.191 Å in $RCq^{end\text{-}on}$). As a result, the N-pyridine trans to the two hydroxyl groups is no longer bound to the manganese center, which preserves the six-coordination, in a trigonal prismatic-like geometry. This peculiar feature is found for both $I_{OHOH}q$ and $I_{OHOH}d$, but not for $I_{OHOH}s$. In the $I_{OHOH}s$ geometry the two hydroxo moieties are not symmetrically bound to Mn (Mn-O1 = 1.918 Å, Mn-O2 = 2.311 Å) and the characteristic position of the axial Py ring stacking parallel to one of the equatorial Py rings is observed (note that $I_{OHOH}s$ is geometrically similar to the $TSIs_{symm}$ and $RC'q^{end\text{-}on}$ structures).

This finding suggests that the formation of the Mn dihydroxo species could take place alternatively via an asymmetric O-O bond cleavage of the H_2O_2. The energy profile for this process is depicted in Figure 5.

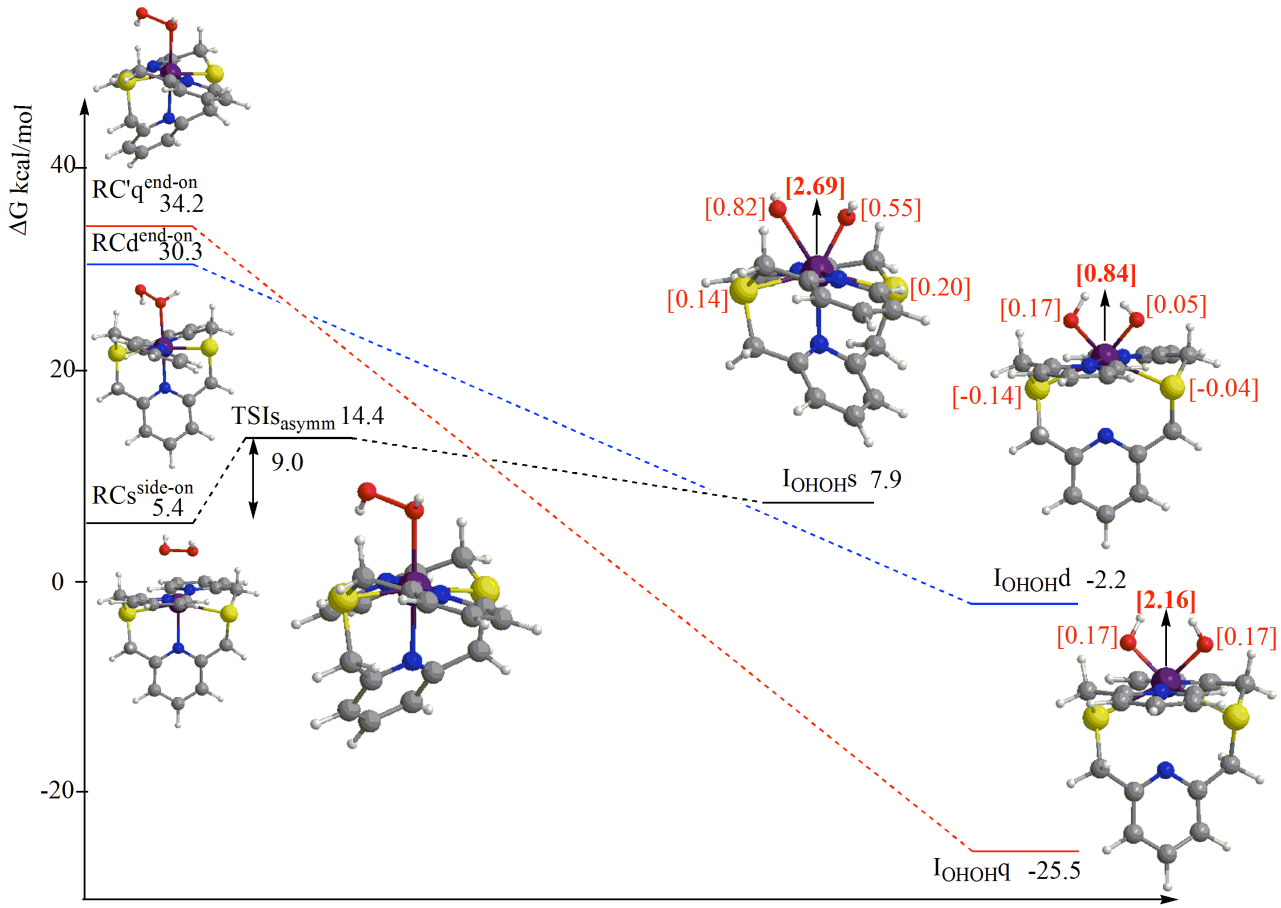

Figure 5. Energy profile of the manganese dihydroxo intermediate formation via an asymmetric O-O bond breaking for sextet (black), quartet (red) and doublet (blue) spin states. The sum of the Gibbs free energies of the separate reactants ($[MnS_2Py_3]^{2+}$ + H_2O_2) is taken as the zero reference energy. Values in square brackets are spin densities (based on Multiple Derived Charges (MDC-q) analysis) calculated on Mn, S and O atoms.

Similar to Figure 4, the energy profile shows that the sextet state is the lowest spin state for the reactant complex $RCs^{end\text{-}on}$ until the transition state $TSIs_{asymm}$, lying 14.4 kcal/mol above the separate reactants, is reached with an activation energy barrier of only 9.0 kcal/mol. In the quartet and doublet energy profiles no transition states have been found, indicating that the asymmetric O-

O bond breaking occurs immediately from the corresponding reactant complexes. A spin crossover from the sextet to the quartet state occurs on the path to the most stable dihydroxo complex $I_{OHOH}q$. The transition state $TSIs_{asymm}$ structure is shown in Figure S6 in the SI.

From these results, we conclude that the O-O bond cleavage in H_2O_2 leading to the Mn dihydroxo species is highly exothermic (ΔG=-25.5 kcal/mol with respect to the free reactants) and it takes place asymmetrically, through a transition state located on the sextet spin state followed by a spin crossover from the sextet to the quartet spin state, with a relatively low activation barrier (9.0 kcal/mol). The removal of the axial pyridine ligand is a crucial factor for stabilizing the dihydroxo species. A special role of the axial ligand has also been reported in the literature, for instance, the O-O bond activation in acylperoxo complexes of [(Salen)Mn(III)L],[67] the H_2O_2 activation by an Mn(III) corrolazine complex,[68] and the nucleophilic reactivity of a nonheme manganese(III)-peroxo complex.[69]

Asymmetric O-O bond cleavage of H_2O_2 could also lead to the generation of the Mn monohydroxo species. The energy profile for the formation of the monohydroxo intermediate is shown in Figure 6, where the monohydroxo intermediate structures are in the sextet, quartet and doublet spin states. The main geometrical parameters are displayed in Figure S7 in the SI.

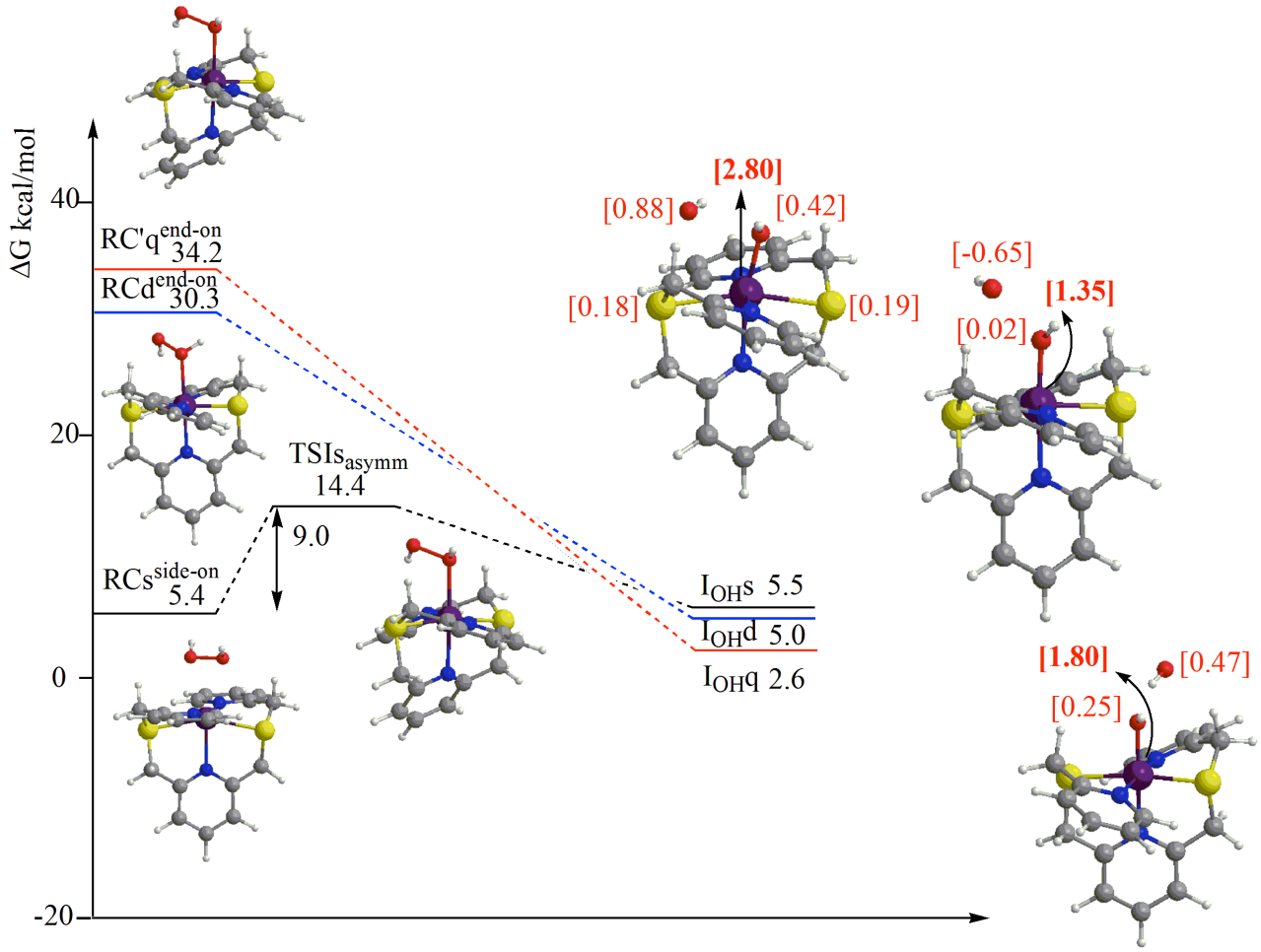

Figure 6. Energy profile of the manganese monohydroxo intermediate formation reaction for sextet (black), quartet (red) and doublet (blue) spin states. The sum of the Gibbs free energies of the separate reactants ($[MnS_2Py_3]^{2+}$ + H_2O_2) is taken as the zero reference energy. Values in square brackets are spin densities (based on Multiple Derived Charges (MDC-q) analysis) calculated on Mn, S and O atoms.

The energy profiles show that the sextet state is always the lowest spin state. The O-O bond breaking leads to the same transition state $TSIs_{asymm}$ as shown in Figures 5 and S6 with the same activation energy of 9.0 kcal/mol (14.4 kcal/mol above the separate reactants). This finding substantiates both the occurrence of the O-O bond breaking in the sextet spin state and the

formation of the dihydroxo complex due to a geometrical rearrangement process that triggers the spin crossover from sextet to quartet. In the monohydroxo intermediate formation, the sextet spin state profile remains at lower energy than the doublet and quartet spin states during the major part of the reaction. Both the doublet and the quartet are very reactive paths leading to the Mn monohydroxo species formation in a barrierless process. The doublet and quartet monohydroxo complexes, I_{OH}d and I_{OH}q, are more stable than I_{OH}s by 0.5 and 2.9 kcal/mol, respectively, with the quartet I_{OH}q being the most stable Mn monohydroxo species, which indicates that a spin crossover from the sextet to the quartet should occur at the vicinity of the final product geometry. Note that the octahedral geometry is retained in I_{OH}q. The geometry of I_{OH}s shows that the OH in the second coordination sphere is not at a very large distance from Mn (Mn-OH = 2.955 Å). A direct comparison between Figures 5 and 6 shows that although the activation energy barrier for both the quartet monohydroxo I_{OH}q and dihydroxo I_{OHOH}q formation is the same (9.0 kcal/mol), since the same $TSIs_{asymm}$ is involved, the quartet monohydroxo I_{OH}q formation reaction is endothermic by only 2.6 kcal/mol compared to the highly exothermic I_{OHOH}q formation (-25.5 kcal/mol). Overall, these results support the Mn dihydroxo species in the quartet state as the thermodynamically favored intermediate.

The O-O bond breaking in H_2O_2 induced by $[MnS_2Py_3]^{2+}$ complex can be analyzed in detail by comparing the electronic structures of RCs $^{side\text{-}on}$ and I_{OH}s, as depicted by the simplified bonding scheme in Figure 7, where evolution of the Mn 3d orbitals and σ* H_2O_2 orbital from $RCs^{side\text{-}on}$ to I_{OH}s can be followed.

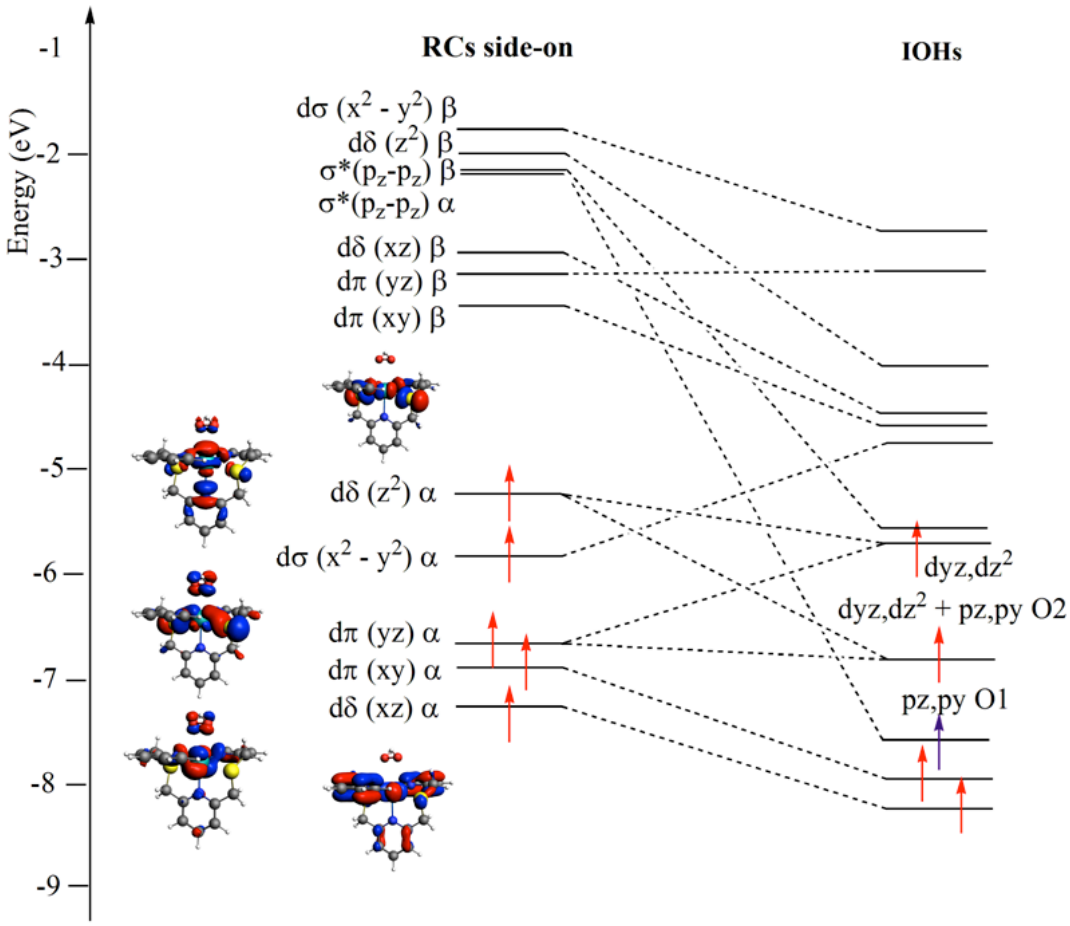

Figure 7. Simplified bonding scheme for the H_2O_2 interactions in $[MnS_2Py_3]^{2+}$ leading to I_{OH}s. O1 denotes oxygen atom of non-coordinating OH, O2 is the oxygen atom of the OH bonded to Mn. The σ, π and δ symmetry labels refer to the $[MnS_2Py_3]^{2+}$ axis system (the axial N atom ligand and the incoming H_2O_2 substrate lies along the y axis, the equatorial S atoms ligand along the z axis, and the equatorial N atoms ligand along the x axis).

In Figure 7 we see that the energy of the five Mn 3d singly occupied α-spin orbitals is lower than that of the empty H_2O_2 σ* (α- and β-spin) orbitals in $RCs^{side\text{-}on}$. In the Mn 3d singly occupied α-spin set, the lowest dδ(xz) has mainly metal character, whereas dπ(xy) and dπ(yz) are pushed up in energy by antibonding interaction with filled H_2O_2 π* orbitals (with a contribution of 6%, and 12%, respectively). Remarkable S ligand atoms character can be found in dπ(yz) (16% $3p_z$ S + 15% $3p_z$

S) and dδ(z^2) (11% $3p_z$ S + 11% $3p_z$ S), while dσ(x^2-y^2) exhibits axial N ligand (antibonding) contribution (12% $2p_y$ N). The electronic structure of $RCs^{side\text{-}on}$ accounts for the spin density distribution described in the previous section. Evolution of $RCs^{side\text{-}on}$ towards I_{OH}s leads to the electronic structure also depicted in Figure 7. In I_{OH}s one of the five α-spin unpaired electrons in $RCs^{side\text{-}on}$ now occupies a $2p_z/2p_y$ hybrid orbital localized on the oxygen atom of the non-coordinating OH (O1, blue arrow in Figure 7), and one electron a bonding Mn dyz/dz^2 – O2 $2p_z/2p_y$ orbital (O2 denotes the oxygen atom of the bonded OH). The remaining three α-spin unpaired electrons are mainly localized on Mn 3d orbitals. A total of "one electron and half" (roughly two electrons) is transferred from Mn to H_2O_2 to form a non-coordinating OH radical and a bond order of 1/2 between Mn and the second OH. Very interestingly, the empty β-spin $2p_z/2p_y$ counterpart of the O1 orbital represents the LUMO and it is very close in energy to the singly occupied α-spin Mn dyz/dz^2 (also containing substantial ligand S atom contributions) HOMO (ΔE = 0.11 eV). A spin flip transition can easily occurs where the Mn dyz/dz^2 α-spin electron transfers to the O1 $2p_z/2p_y$ orbital with a β-spin, accounting for a spin crossover from sextet to quartet in the complex. We should notice that the α-spin electron undergoing the transition is partially delocalized on the S ligand atoms, which experience then a loss of α-spin density in spin crossover. Occupation of the O1 $2p_z/2p_y$ orbital with the β-spin electron allows bonding of the non-coordinating OH with Mn, coupled with a geometry rearrangement resulting in I_{OHOH}q, where the bond order between the Mn and each OH can be considered 1/2.

The nature of the dihydroxo and monohydroxo species is clearly visualized in the spin density distribution. In I_{OHOH} in the sextet spin state, roughly three unpaired electrons localize on the metal (2.69), one unpaired electron on one oxygen atom of H_2O_2 (0.82), and 1one unpaired electron delocalizes on S donor atoms of the ligand (0.20,0.14) and on the other oxygen atom of H_2O_2 bonded to Mn (0.55), which leads to an overall electronic structure in the sextet state and to a formal high-spin Mn(IV) (five α-spin unpaired electrons on the complex with roughly three unpaired electrons on Mn) (see Fig.5). Interestingly, in the sextet state the spin density distribution

in the intermediate I_{OH} is very similar to that in I_{OHOH} (compare Figure 5 and 6), thus suggesting that the H_2O_2 dissociation in the sextet spin state invariably leads to a non-coordinating OH radical. A different situation is found in the quartet spin state. In the I_{OHOH}, three unpaired electrons are delocalized over the Mn atom (2.16) and the two oxygen atoms of the two hydroxyl moieties (0.17 and 0.17), a spin distribution roughly corresponding to a formal Mn(IV) (about three unpaired electrons on Mn, with two α- and β-spin electrons each involved in the bonding of one OH group) (see Fig.5 and 7). In I_{OH} the spin density on Mn and hydroxyl bonded to it is close to two, which can be similarly assigned to a Mn(IV), with roughly the third unpaired electron localized on the oxygen atom of the non-coordinating OH (0.47) (Fig. 6). Notably, I_{OH} in the quartet state bears a much less radical character than that in I_{OH} in the sextet spin state. Finally, in the I_{OHOH} in the doublet state, one unpaired electron is delocalized on the Mn center (0.84) and on one oxygen atom of an hydroxyl group (0.17) (see Fig.5), whereas in I_{OH} an antiferromagnetically coupled spin between the non-coordinating OH oxygen atom (about one beta-spin unpaired electron) and Mn (two alpha-spin unpaired electrons) has been found (see Fig. 6).

Formation of the Mn(IV) oxo species: exploring the ping-pong reaction channel

Finally we investigated the formation of the Mn(IV) oxo species plus a water molecule as the first dismutation products via the I_{OH} and I_{OHOH} intermediates calculated for each spin state. The energy profiles are shown in Figure 8 and the transition states and intermediate structures in the sextet, quartet and doublet spin states together with the main geometrical parameters are reported in Figure S8 in the SI.

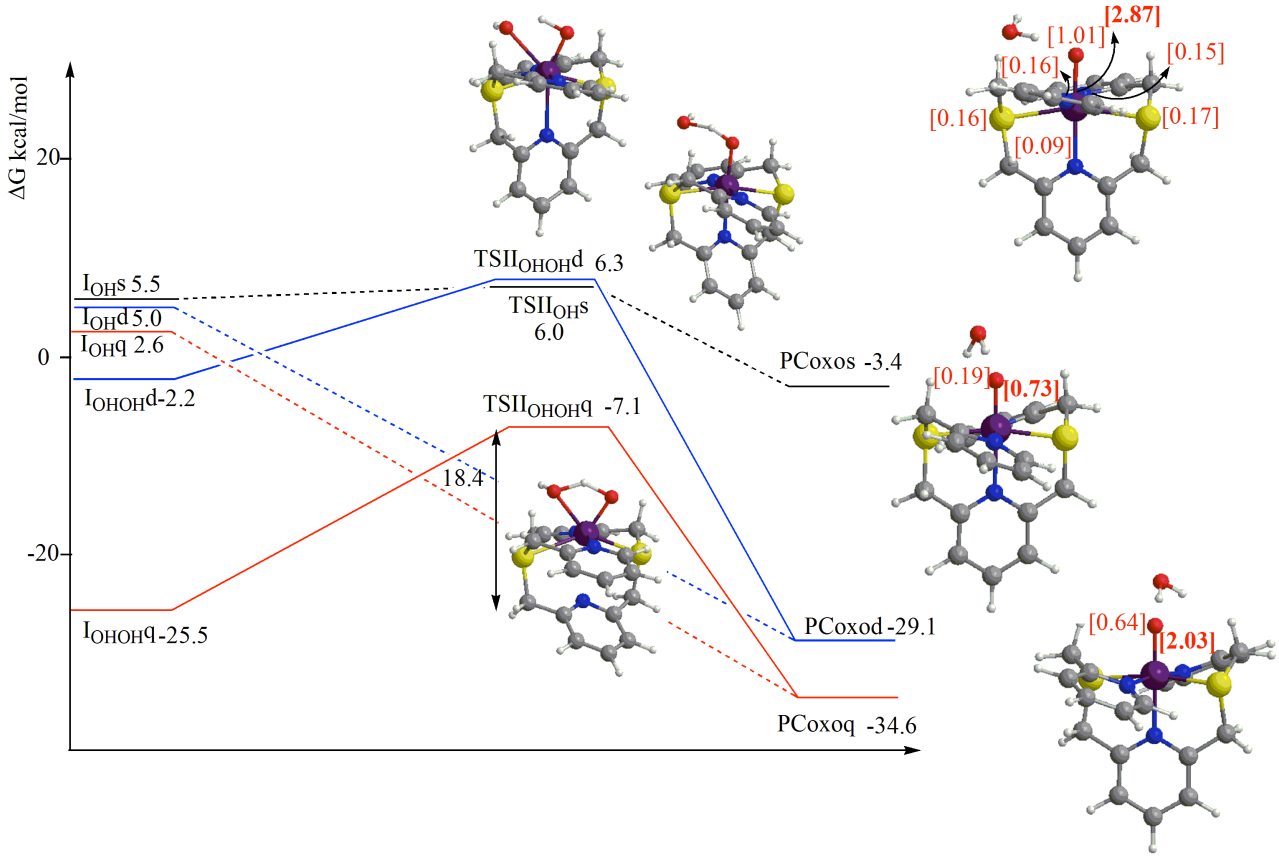

Figure 8. Energy profile for the manganese oxo intermediate formation from the manganese monohydroxo intermediate for sextet (black), and from the manganese dihydroxo/monohydroxo intermediate for quartet (red) and doublet (blue) spin states. Dashed lines connect species involving monohydroxo intermediates; solid lines connect species involving dihydroxo intermediates. Values in square brackets are spin densities (based on Multiple Derived Charges (MDC-q) analysis) calculated on Mn, S, N and O atoms.

Starting from the Mn dihydroxo intermediates in the sextet ($I_{OHOH}s$), quartet ($I_{OHOH}q$) and doublet ($I_{OHOH}d$) spin states, the formation of the corresponding Mn oxo species plus a water molecule is induced by approaching a hydrogen atom of one OH group to the vicinal oxygen atom of the second OH group. During this process, in the sextet spin state, one of the coordinated OH groups readily

dissociates from Mn leading to the more stable monohydroxo species, thus confirming that the dihydroxo species is not a viable intermediate in this spin state. Therefore, for the sextet spin state profile we start from I_{OH}s. From the monohydroxo intermediates in the sextet (I_{OH}s), quartet (I_{OH}q) and doublet (I_{OH}d) spin state, the hydrogen transfer is achieved by approaching the hydrogen atom of the OH group bound to Mn towards the non-coordinating hydroxide. The formation of the Mn oxo species plus a water molecule via the monohydroxo intermediate would be a barrierless process in the quartet and doublet spin states and it requires only 0.5 kcal/mol in the sextet. However, the energy profiles show that the quartet state (via both the I_{OHOH} and I_{OH} intermediates) is always the lowest spin state and the sextet is the highest.

For the ping-pong mechanism via the Mn(IV) dihydroxo intermediate, a relatively low activation barrier is calculated on the doublet spin state (8.5 kcal/mol with respect to I_{OHOH}d), leading to a very stable product PC_{oxod} (29.1 kcal/mol below the separate reactants), but the excitation of the I_{OHOH} complex from the quartet to the doublet state would require 23.3 kcal/mol. The transition state for the hydrogen migration is calculated on the quartet spin state ($TSII_{OHOH}$q) with an activation barrier of 18.4 kcal/mol. The PC_{oxoq} product is more stable than the separate reactants by 34.6 kcal/mol. This reaction is exothermic (PC_{oxoq} is more stable than I_{OHOH}q by 9.1 kcal/mol) but the activation energy barrier is relatively high (18.4 kcal/mol) and this would represent the rate-determining step for the whole first dismutation reaction leading to the Mn oxo species. Therefore, the intermediate I_{OHOH}q can be considered as an "energetic trap" on this reaction path, making the ping-pong mechanism much less efficient than the pathway via monohydroxo intermediates.

These results clearly suggest that the first dismutation reaction with the $[MnS_2Py_3]^{2+}$ complex cannot be simply described with the classical ping-pong mechanism leading to the formation of a Mn oxo intermediate and a water molecule, but an alternative one-step mechanism, leading to the formation of a stable Mn dihydroxo intermediate via a spin crossover from a sextet to a quartet spin state is also viable. Mn dihydroxo complexes are rare but not unknown in the literature. For example, a robust Mn(IV) dihydroxo complex with a rigid, cross-bridged, cyclam ligand, 4,11-

dimethyl-1,4,8,11-tetraazabicyclo[6.6.2]hexadecane, $[Mn(Me_2EBC)(OH)_2]^{2+}$, has been reported by Busch and coworkers[70] as the first thoroughly characterized monomeric Mn(IV) complex containing a pair of hydroxo ligands constituting the activated form of the oxidation catalyst with hydrogen abstracting ability. Evidence for a mononuclear Mn(IV) complex with two hydroxide ligands in a cis arrangement has been reported by Costas and coworkers.[71] The authors show the ability of the Mn(IV) complex $[Mn(^{H,Me}Pytacn)(OH)_2]^{2+}$ (Pytacn = 1-(2-pyridylmethyl)-4,7-dimethyl-1,4,7-triazacyclononane) to abstract a hydrogen atom from C-H bonds of several substrates. Further evidence supporting a mononuclear Mn(II) catalyst for H_2O_2 disproportionation was obtained by Smith and coworkers[72)] with a pyridinophane complex $[Mn(Py_2N_2)(H_2O)_2]^{2+}$. A catalytic cycle consistent with experimental data was proposed which involves the formation of a hydroperoxo intermediate $[Mn(Py_2N_2)(H_2O)(O_2H)]^{+}$ with H_2O and O_2H^- in a cis arrangement.

The reactivity of the Mn mono oxo intermediate with the second H_2O_2 substrate molecule in the second dismutation reaction can be predicted on the basis of the electronic structure and spin density distribution in PC_{loxo} species. It is instructive to compare the electronic structures of PC_{oxos} and PC_{oxoq}, which are depicted as simplified MO diagrams in terms of basic bonding pattern of Mn-O in Figure 9. The two complexes feature Mn(IV)-oxo units in a octahedral geometry with the same ligand and consequently we can understand the variations in promoting hydrogen-abstraction from H_2O_2 on the basis of the exchange-field strength depending on the spin state.[73]

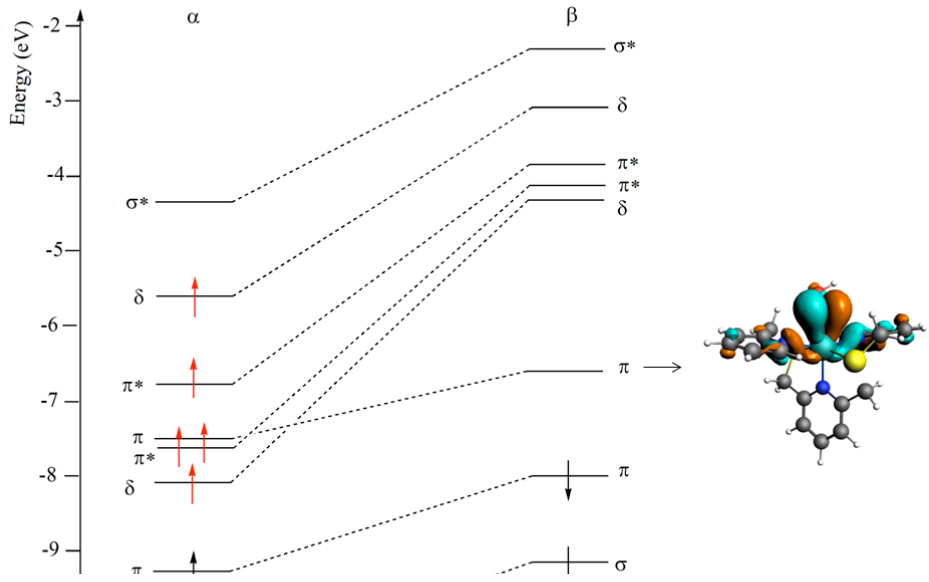

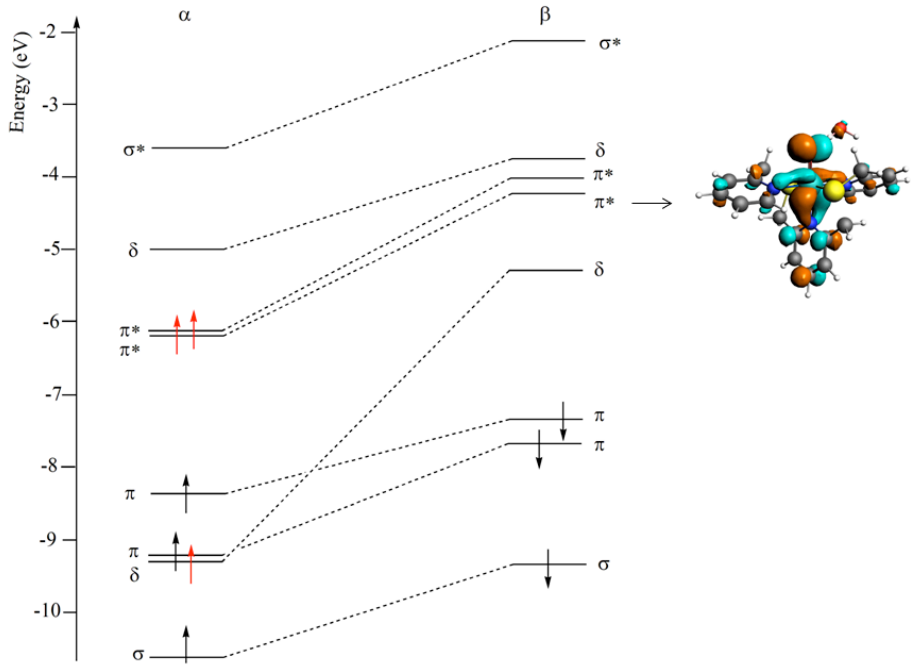

Figure 9. Valence orbital level diagram for the PC_{Ioxo} species: top) sextet spin state (PC_{oxos}); bottom) quartet spin state (PC_{oxoq}). Only Mn-O states are illustrated for simplicity. Unpaired electrons are represented with red arrows.

As illustrated in ref.s [74,75], the basic bonding pattern of a M-O unit is similar to that of dioxygen: there are three occupied bonding orbitals (pdσ, $pd\pi_x$ and $pd\pi_z$, see the black up and down arrows in the α- and β-spin orbitals in Figure 9), and there are two unpaired electrons (red arrows) in the antibonding $dp\pi^*_x$ and $dp\pi^*_z$. Notation pdσ and pdπ is used here for the low-lying bonding combinations of O 2p with Mn 3p orbitals, which are nominally "oxygen levels" (leading p contribution), whereas dpσ* and dpπ* denote the higher-lying antibonding orbitals, which are

nominally "d orbitals" (leading d contribution). The difference of the MnO^{2+} electronic structure with the basic O_2-type bonding scheme is in the presence of the two nonbonding 3d orbitals on Mn of δ symmetry with respect to the Mn-O axis (here the y axis), the dz^2 and dxz orbitals. They contain two unpaired electrons (all unpaired electrons are denoted with red arrows) which, with the two unpaired electrons in the π* levels, add up to four. The fifth unpaired electron leading to the sextet spin state resides in the bonding $pd\pi_x$ (Figure 9 top)). The sextet spin configuration $(pd\sigma\ \alpha)^1(pd\sigma\ \beta)^1(pd\pi_z\ \alpha)^1(pd\pi_z\ \beta)^1(pd\pi_x\ \alpha)^1(pd\pi_x\ \beta)^0(dp\pi^*_x\ \alpha)^1(dp\pi^*_z\ \alpha)^1(dz^2\ \alpha)^1(dxz\ \alpha)^1$ corresponds to a Mn-O bond order of 3/2. Note that this electronic configuration is in an excited state, with the empty $pd\pi_x\ \beta$ (π bonding) orbital lying at lower energy than that of the singly occupied $dz^2\ \alpha$ (δ nonbonding orbital). The excited-state reactivity model has been previously proposed in the literature for understanding hydrogen-atom transfer for $[Mn^{IV}(O)(N4py)]^{2+}$ (N4py = N,N-bis(2-pyridylmethyl)-N-bis(2-pyridyl)methylamine pentadentate ligand) and related Mn^{IV}-oxo complexes.[76-78] This high-spin configuration reverts to the quartet spin configuration $(pd\sigma\ \alpha)^1(pd\sigma\ \beta)^1(pd\pi_z\ \alpha)^1(pd\pi_z\ \beta)^1(pd\pi_x\ \alpha)^1(pd\pi_x\ \beta)^1(dp\pi^*_x\ \alpha)^1(dp\pi^*_z\ \alpha)^0(dxz\ \alpha)^1$,where both the pdπ (π bonding) orbitals are occupied and the δ nonbonding is empty, leading to a Mn-O bond order of 2 and getting stabilized by 31.2 kcal/mol (Figure 8). In the sextet spin state the lowest-lying vacant orbital is $pd\pi_x\ \beta$, which is bonding between the Mn dxy and O p_x orbitals, whereas in the quartet state the lowest-lying vacant orbital is $dp\pi^*_x\ \beta$, which is antibonding between the Mn dxy and O p_x orbitals (see Figure 9). The energy of the lowest vacant orbital and its oxygen p orbital contribution are the two important factors in predicting the electrophilicity of a MO^{2+} moiety. Generally speaking, the lower the acceptor orbital lies in energy and the higher the % oxygen p orbital contribution is, the more electrophilic the MO^{2+} will be: in our case they are both in favor of a large electronic donation from the H-OOH bond into the MnO^{2+} acceptor orbital. Based on these two factors, a much higher reactivity of the Mn oxo intermediate in the sextet spin state is expected, since both the energy of the acceptor $pd\pi_x\ \beta$ orbital is lower (-6.65 eV vs. -4.19 eV for $dp\pi^*_x\ \beta$ in the quartet state) and the % oxygen p_x orbital contribution is higher (59% vs. 15% for $dp\pi^*_x\ \beta$ in the

quartet state). The spin density distribution resulting from electronic structure in PC_{oxoI} intermediates is shown in Figure 8. In PC_{oxos} the spin density on the metal/ligand system is overall close to four, with roughly three unpaired electrons on the single metal, assigned to high-spin Mn(IV), and with the fifth unpaired electron localized on the oxo oxygen, leading to an overall electronic structure in the sextet state. In PC_{oxoq} the spin density is 0.64 on the oxo oxygen and close to two on Mn which sums up to three unpaired electrons on the whole complex. Finally, in PC_{oxod} one unpaired electron is delocalized over the Mn center and the oxo oxygen. In Table S1 in the SI the Multiple Derived Charges (MDC) spin densities[56] are reported for all the species (initial complexes (IC), reactant complexes (RC_I), intermediates (I_{OHOH}, I_{OH}) and product complexes (PC_{Ioxo})) involved in the first dismutation reaction.

In conclusion, the $[MnS_2Py_3]^{2+}$-catalyzed first dismutation reaction can be described as a multichannel process combining both ping-pong and dihydroxo pathways. The competing channels have different spin states: the sextet reaction pathway corresponds to a ping-pong mechanism, the doublet should allow both a ping-pong and a dihydroxo mechanism, and the quartet would preferably follow a dihydroxo mechanism. Importantly, the two mechanistic channels are characterized by different coordination geometries of the involved species: octahedral in the ping-pong route, trigonal prismatic in the dihydroxo path, suggesting that the reaction mechanism is controlled by spin transitions triggered by Mn coordination switching and vice versa. Both the Mn oxo (sextet and quartet spin state) and the Mn dihydroxo (quartet spin state) species have spin density on oxygen, a factor that has been found to be crucial in promoting hydrogen abstraction.[79]

Second dismutation reaction

A manganese(IV) dihydroxo compound in a quartet spin state has been obtained as a thermodynamically stable product from the first dismutation reaction. The second dismutation reaction should convert hydrogen peroxide to two water molecules and dioxygen. The second dismutation reaction has been studied for the quartet and doublet spin states according to this mechanism. However, if the catalyst does not enter the dihydroxo route, namely if the monohydroxo immediately converts into the oxo intermediate, then the ping-pong channel should also be viable for the quartet spin state. Since the ping-pong mechanism is preferred for the sextet spin state, we start in the second dismutation reaction from the oxo intermediate which should convert hydrogen peroxide to one water molecule and dioxygen. Finally, we note that for the doublet spin state, the ping-pong mechanism is also feasible and, since the oxo intermediate is kinetically accessible and thermodynamically more stable than the dihydroxo intermediate, we will consider this as an alternative reactant complex for the second dismutation reaction. Summarizing, on the basis of our findings, two possible mechanistic channels are considered, as shown in Scheme 2: firstly, the ping-pong channel (for the sextet, quartet and doublet spin states) which, starting from $PC_{oxo}s$, $PC_{oxo}q$ and $PC_{oxo}d$, leads to the conversion of H_2O_2 into H_2O and O_2 with simultaneous deoxygenation of the Mn complex; secondly, the dihydroxo channel (for the quartet and the doublet spin states) which, starting from $I_{OHOH}q$ and $I_{OHOH}d$, converts H_2O_2 into two H_2O molecules and O_2 with simultaneous dehydroxylation of the metal complex. In the latter case, a hydroxo-hydroperoxo intermediate retaining the trigonal prismatic coordination should be involved.[72] In the ping-pong channel, the water molecule formed as a product of the first dismutation reaction is included in the energy profile calculations for a direct comparison with the dihydroxo channel energy profile.

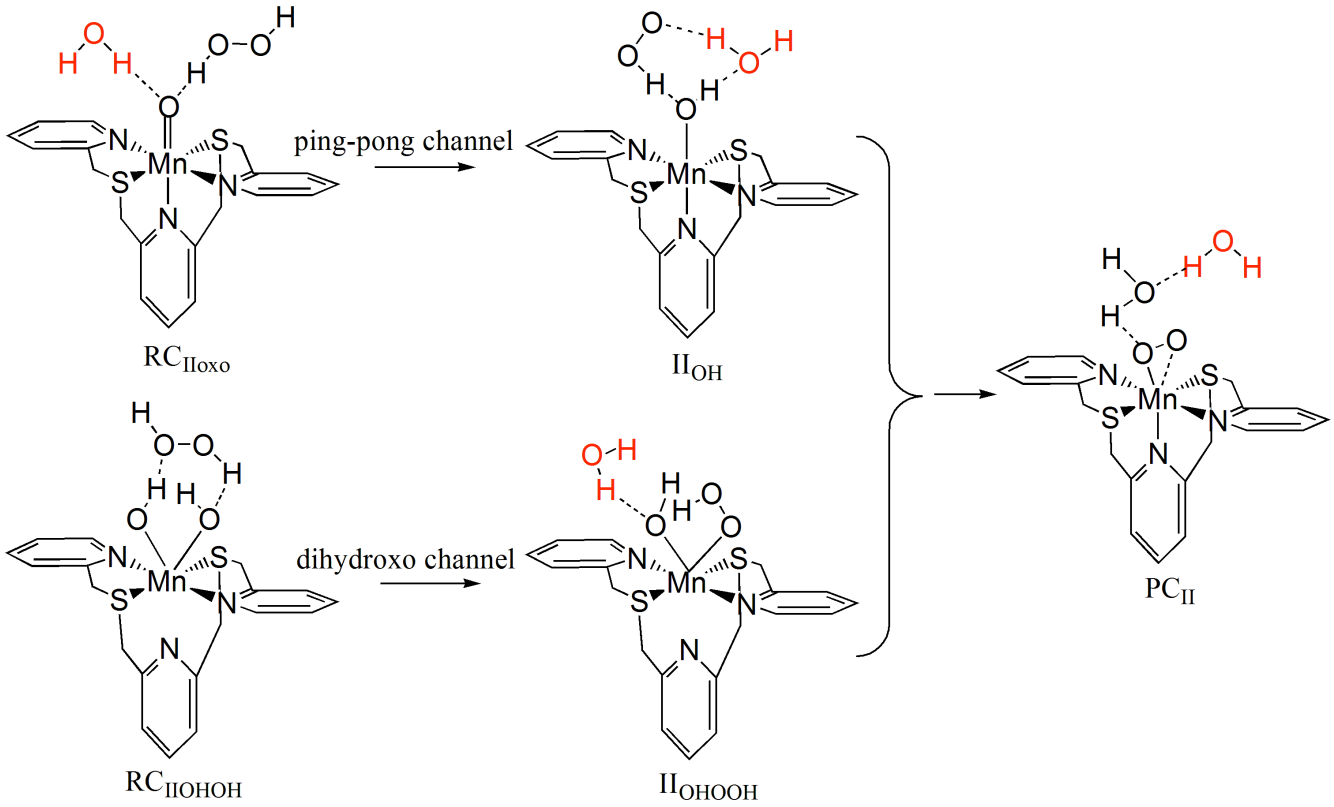

Scheme 2. Reactant complexes, intermediates and the common product complex from the ping-pong (top) and dihydroxo (bottom) mechanisms for the second dismutation reaction of hydrogen peroxide catalyzed by $[MnS_2Py_3(OH)_2]^{2+}/[MnS_2Py_3O]^{2+}(H_2O)$; ping-pong channel: RC_{IIoxo} represents the reactant complex from the oxo intermediate (PC_{Ioxo}) and II_{OH} the Mn monohydroxo intermediate (plus a free hydroperoxide moiety); dihydroxo channel: RC_{IIOHOH} represents the reactant complex from I_{OHOH} intermediate, and II_{OHOOH} the Mn hydroxo-hydroperoxo intermediate. PC_{II} represents the same final product complex, which represents the Mn(II) initial catalyst with a coordinated O_2 product molecule plus two product water molecules.

Due to the complex picture of the second dismutation reaction as a multichannel process with different spin states, we present our findings for each spin state separately.

All of the reaction profiles for the three different spin states and for the two pathways (ping-pong

and dihydroxo) are compared in Figure 10, where the energy of the separate reactants $I_{OHOH}q$ + H_2O_2 and $PC_{oxo}q$ + H_2O_2 are taken as zero reference energy.

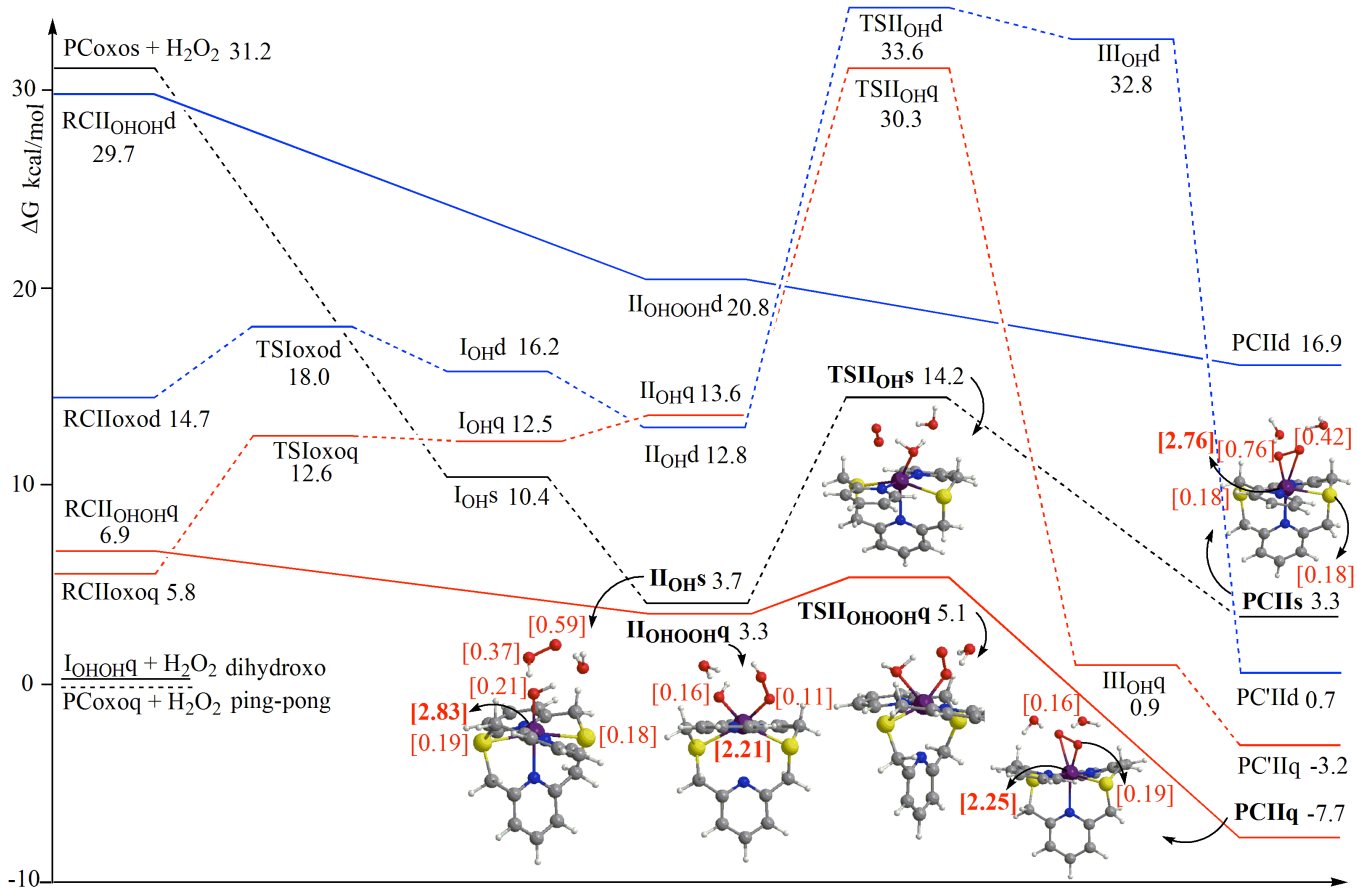

Figure 10. Energy profiles for the second dismutation reaction on the sextet (black), quartet (red) and doublet (blue) spin states. Dashed lines are used for ping-pong pathways, solid lines for dihydroxo pathways. The sum of the Gibbs free energies of the separate reactants ($I_{OHOH}q + H_2O_2$ and $PC_{oxo}q + H_2O_2$) are taken as zero reference energy. Geometrical structures and spin density on Mn, S and O atoms (values in square brackets, based on Multiple Derived Charges (MDC-q) analysis) of the most relevant species are also shown.

Two very interesting features can be observed from Figure 10: firstly, the strong hydrogen-abstraction ability of $PC_{oxo}s$ is responsible for the sextet energy profile to be the lowest energy path for the ping-pong route. A second spin transition from quartet to sextet occurs after the TSIoxoq has been reached with an activation energy barrier of 6.8 kcal/mol for the first hydrogen abstraction from H_2O_2. Secondly, the high reactivity of $I_{OHOH}q$ results in a very low barrier along the quartet energy profile for the dihydroxo route. These two features make the ping-pong path on the sextet spin state and the dihydroxo path on the quartet spin state the two minimum energy channels. The rate determining step of the second dismutation reaction is the second hydrogen abstraction from H_2O_2, namely by $TSII_{OHOH}q$ and $TSII_{OH}s$ in Figure 10. However, the activation energy barrier along the quartet energy profile is much lower than that along the sextet (1.8 vs. 10.5 kcal/mol, respectively).

Sextet state reaction pathway.

As mentioned above, only the ping-pong mechanism has been considered for the sextet state and a stepwise path has been calculated as depicted in Figure 10 (black dashed line energy profile) . The optimized geometries for the involved species can be found in Figure S9 in the SI. Despite many attempts, we failed to find a stable reactant complex $RCII_{oxo}s$ starting from $PC_{oxo}s$ and a vicinal

H_2O_2. The two reactants immediately form the intermediate species I_{OH}s (see Figures 10 and S9) which is stabilized by 20.8 kcal/mol with respect to the sum of the energies of the separate reactants PC_{oxo}s + H_2O_2, thus confirming the strong hydrogen abstraction ability of the Mn(IV)oxo moiety. Intermediate I_{OH}s can be described as a monohydroxo Mn complex with a hydroperoxo group hydrogen-bonded to Mn-OH as a hydrogen-acceptor species, with a OH-OOH distance of 1.741 Å. However, many hydrogen-bonded configurations can be calculated for H_2O, OOH and OH in this species, and among them, the structure denoted II_{OH}s in Figures 10 and S9 is more stable than I_{OH}s by 6.7 kcal/mol. Importantly, II_{OH}s shows the hydroperoxo group hydrogen-bonded to Mn-OH as the hydrogen-donor species, with a OOH-OH distance of 1.406 Å. Note that the OOH peroxide position in II_{OH}s is a suitable starting point for the second proton transfer. In the OOH hydrogen approach to OH-Mn, the energy goes uniformly uphill and neither a transition state nor a product complex with a water molecule bound to Mn could be found, thus signaling the weak hydrogen abstraction ability of the Mn-OH complex. Instead a transition state for the second proton transfer can be reached by rotating the peroxide moiety to allow an oxygen atom interaction with Mn. The $TSII_{OH}$s geometry, depicted in Figure S9, is characterized by an almost completely abstracted hydrogen (OO-H distance = 1.554 Å, OOH-OH distance = 1.045 Å), a shortening of the O-OH bond (1.336 Å) and an early stage formation of the OO-Mn bond with a distance between O and Mn of 2.557 Å. The $TSII_{OH}$s structure leads directly to the product complex PC_{II}s (Figures 10 and S9). In the final complex the dioxygen molecule is coordinated to the Mn center approximately in an end-on mode (Mn-O1 = 1.937 Å, Mn-O2 = 2.449 Å, O1-O2 = 1.334 Å). The energy barrier corresponding to $TSII_{OH}$s is 10.5 kcal/mol and the reaction is endothermic by 3.3 kcal/mol with respect to separate reactants PC_{oxo}q + H_2O_2 and exothermic by 27.9 kcal/mol with respect to separate PC_{oxo}s + H_2O_2.

The electronic structure analysis of II_{OH}s shows that the lowest α-spin vacant orbital can be described as a σ* orbital between the oxygen atom of the OH (8% p_y) and Mn (27% dxy + 20 dx^2-y^2) which is a suitable acceptor orbital in the hydrogen abstraction reactivity. Both its relatively high

energy (-4.623 eV with respect to -5.268 eV of the lowest β-spin vacant orbital of OOH π* character) and low oxygen p orbital contribution (8%) are responsible for the calculated 10.5 kcal/mol energy barrier. The spin density distribution resulting from its electronic structure is shown in Figure 10. The $II_{OH}s$ has four unpaired electrons on the metal complex (roughly three on Mn and one delocalized over the S donor atoms and OH oxygen atom), and one unpaired electron on OOH moiety, the latter showing a radical character, which leads the overall species to a sextet spin state. In conclusion, in the sextet reaction channel a ping-pong mechanism would be feasible, with the second proton transfer being the rate-determining step of the second dismutation reaction.

Quartet state reaction pathway.

It was found that the reaction in the quartet spin state could proceed through a dihydroxo mechanism. When the second H_2O_2 substrate approaches the dihydroxo intermediate $I_{OHOH}q$, two possible conformations for the reactant complex $RCII_{OHOH}$ can be obtained, based on the two hydrogen bonds which can be formed between the hydrogen atoms of H_2O_2 and the two OH groups coordinated to Mn. In the first configuration, denoted as $RCII_{OHOH}q$, H_2O_2 acts as a proton donor for one bond and as a proton acceptor for the other. In the second configuration, denoted as $RC'II_{OHOH}q$, H_2O_2 acts as proton donor for both bonds. The optimized geometries of the two reactant complexes are depicted in Figure S10 in the SI. The most stable reactant complex is $RCII_{OHOH}q$, which is less stable than the sum of the Gibbs free energies of the isolated reactants ($I_{OHOH}q$ + H_2O_2) by 6.9 kcal/mol. The alternative reactant complex in the quartet spin state, $RC'II_{OHOH}q$, is 12.0 kcal/mol higher in energy than the free reactants. In the $RCII_{OHOH}q$ structure an incipient hydrogen abstraction from H_2O_2 is observed (H_2O_2 O-H = 1.015 Å), and a simultaneous elongation of the hydrogen abstracting HO-Mn bond (1.872 Å). From $RCII_{OHOH}q$, through a barrierless reaction (red solid line energy profile in Figure 10), a Mn(IV) hydroxo hydroperoxo intermediate complex is formed ($II_{OHOOH}q$ in Figure 10 and S10) which is more stable than

$RCII_{OHOH}q$ by 3.6 kcal/mol. A water molecule is released with the hydroperoxo group substituting the leaving H_2O ligand in the Mn coordination sphere. Note that the Mn coordination features in $I_{OHOOH}q$ (in particular the elongated Mn-N pyridine bond trans to the two hydroxo ligands leading to the trigonal prismatic coordination geometry in $I_{OHOH}q$) are retained (see Figure S10). Starting from the geometry of $I_{OHOOH}q$, the $TSII_{OHOOH}q$ structure can be obtained by forcing the H atom of the hydroperoxide ligand towards the oxygen of the hydroxide ligand. In the $TSII_{OHOOH}q$ geometry (see Figure S10), the hydrogen has been largely transferred to OH (OO-H distance = 1.437 Å, HO-H distance = 1.070 Å), with a simultaneous shortening of the O-O distance in the hydroperoxide moiety (1.384 Å). The $TSII_{OHOOH}q$ transition state leads to the product complex PCIIq (see Figures 10 and S10) which consists of a dioxygen molecule coordinated to Mn in a end-on fashion (Mn-O1 = 1.815 Å, Mn-O2 = 2.418 Å, O1-O2 = 1.395 Å) and two water molecules hydrogen-bonded to O_2. A very modest amount of energy (1.8 kcal/mol) is needed to activate this step. The PCIIq product complex is more stable than $RCII_{OHOH}q$ by 14.6 kcal/mol and it is also more stable than PCIIs by 11.0 kcal/mol. Our study reveals that the intermediate $I_{OHOH}q$ formed in the first dismutation reaction rapidly evolves to give two H_2O and one O_2 product molecules, with a very low energy cost (dihydroxo mechanism). The lowest α-spin vacant orbital of $II_{OHOOH}q$ has a mainly metal character (13% dxy + 16 dx^2-y^2 + 9% dz^2 + 8% dxz) with a small contribution from the oxygen atom of OH (4% p_z + 2% p_y), interacting in an antibonding fashion. This orbital can be a suitable acceptor orbital in the hydrogen abstraction, with a relatively low energy (-5.284 eV), although the oxygen p orbital contribution (6%) is also low. The $II_{OHOOH}q$ has somewhat more than two unpaired electrons on the metal complex, roughly two on Mn and the remaining delocalized over the OH (0.16) and OOH (0.11) oxygen atoms (see Figure 10).

However, as mentioned above, one may argue that the catalyst could be temporarily deactivated for the ping-pong mechanism if it entered the dihydroxo reaction route in the first dismutation process, due to formation of the thermodynamically stable $I_{OHOH}q$. The issue we want to address now is what

happens if the catalyst does not enter the $I_{OHOH}q$ reaction path but it follows the ping-pong mechanism.

The energy profile for this stepwise path is depicted in Figure 10 as dashed red lines. The optimized geometries of the involved species can be found in Figure S11 in the SI.

The reaction starts with the reactant complex RCIIoxoq which is less stable than the separate reactants $PC_{oxo}q$ + H_2O_2 by 5.8 kcal/mol. The hydrogen abstraction by the Mn-oxo requires an activation energy barrier of 6.8 kcal/mol through a transition state characterized by a very product-like structure (TSIoxoq), leading to intermediate $I_{OH}q$ in Figure 10 and S11. Geometry rearrangement to yield the structure denoted $II_{OH}q$ further destabilizes $I_{OH}q$ by 1.1 kcal/mol, and, as for the sextet, it shows the hydroperoxo group hydrogen-bonded to Mn-OH acting as a hydrogen-donor, with a OOH-OH distance of 1.418 Å. Analogously to the sextet spin route, in the OOH hydrogen approach to OH-Mn, the energy goes uniformly uphill and neither a transition state nor a product complex with a water molecule bound to Mn could be calculated, but, rather, a transition state for the second proton transfer can be reached by allowing an oxygen atom of OOH to interact with Mn. The $TSII_{OH}q$ geometry is depicted in Figure S11 and it is characterized by a very early stage hydrogen abstraction (OO-H distance = 0.997 Å, OOH-OH distance = 2.075 Å), a lengthening of the O-OH bond (1.463 Å) and an early stage formation of the OO-Mn bond with a distance between O and Mn of 2.317 Å. The $TSII_{OH}q$ structure leads to intermediate $III_{OH}q$ with an energy barrier of 16.7 kcal/mol and this step is exothermic by 12.7 kcal/mol. $III_{OH}q$ structure is characterized by a significant geometrical rearrangement with respect to $TSII_{OH}q$, most noticeable the de-coordination of one of the equatorial pyridyl ligands (Mn-N = 3.890 Å). The hydrogen transfer from OOH to OH leads to the product complex PC'IIq, whose structure is very different from that of PCIIq (see Figure S10). In PC'IIq the dioxygen molecule is coordinated in a side-on mode (Mn-O1 = 1.820 Å, Mn-O2 = 1.808 Å, O1-O2 = 1.439 Å), showing the formation of a O_2 – Mn adduct. Overall, the quartet channel seems to be viable in the second dismutation reaction only for the dihydroxo mechanism. To demonstrate that PCIIq represents the initial sextet catalyst plus a

triplet O_2 molecule anti-ferromagnetically coupled, the corresponding structure in the octet spin state, PCIIo, where the initial catalyst and O_2 are ferromagnetically coupled, has been optimized. The geometry is shown in Figure S14 in the SI, where the alternative product complex with a H_2O molecule coordinated to Mn (PC'IIo) has also been calculated. Incidentally, PC'IIo, with the O_2 molecule in the second coordination sphere and thus without magnetic coupling, is more stable than PCIIo by 9.9 kcal/mol. On comparing the PCIIo geometry with that of the initial catalyst shown in Figure 1 (middle), we can see that they are very similar. The high spin of PCIIo is however less stable than the anti-ferromagnetically coupled PCIIq by 1.4 kcal/mol. A single point broken symmetry calculation using the geometry of PCIIo with spin-α density on the metal (five α spin unpaired electrons) and spin-β density on O_2 (two β spin unpaired electrons), resulting in a quartet spin state ("low spin"), has been carried out. The high spin octet configuration is computed to be less stable than the "low spin" broken symmetry configuration by 1.5 kcal/mol, thus showing that PCIIq indeed represents the initial catalyst plus a triplet O_2 molecule anti-ferromagnetically coupled. The spin density distribution in PCIIq, showing roughly three unpaired electrons on the metal and small spin density on O_2 (0.19 and 0.16), indeed supports an anti-ferromagnetically coupled spin between O_2 (two unpaired electrons) and the sextet Mn(II) (five unpaired electrons). Finally, we briefly comment on the lack of reactivity in the hydrogen abstraction for $II_{OH}q$ species in Figure 10. Inspection of its electronic structure reveals that the lowest lying vacant orbital has mainly OOH character, and no suitable acceptor orbitals containing OH contribution are available at low energies.

For the doublet state reaction pathway, we note that the doublet spin state has shown intermediate features between those of the quartet and the sextet reactions. The second dismutation process in the doublet state can in principle proceed via both a ping-pong and a dihydroxo mechanism, since both $PC_{oxo}d$ and $I_{OHOH}d$ are accessible species. However, the energy profiles for both mechanisms are always higher than those for the sextet and quartet spin states, therefore the doublet state reaction pathway seems unfavorable in the second dismutation reaction for both channels. Results for the

second dismutation reaction in the doublet spin state are discussed in detail in the SI (Figures S12 and S13).

Spin density values for all the species involved in the second dismutation reaction can be found in the SI (Tables S2-S5).

Summarizing: the overall $2H_2O_2 \rightarrow 2H_2O + O_2$ dismutation reaction catalyzed by $[MnS_2Py_3]^{2+}$ can occur through two competing channels: the ping-pong mechanism along the sextet and the dihydroxo mechanism along the quartet pathway. Both share the same rate determining step (RDS) in the first dismutation reaction: the O-O bond breaking of H_2O_2 which occurs in the sextet spin state with an activation barrier of 9.0 kcal/mol. In the next subsection we will further explore the RDS to elucidate the role of the explicit solvent, counterion and water (trace amounts) on this activation energy barrier for the first dismutation reaction.

Solvent, counterion and water effects on the O-O bond breaking of H_2O_2

The role of solvent, counterion and trace amount of water in acetonitrile can be important in the H_2O_2 bond breaking process on the sextet spin state in the first dismutation reaction. For this reason we also considered the O-O bond cleavage in the presence of explicit solvent (two acetonitrile molecules), the anion (OTf^-) and traces of water (four H_2O molecules) together with the COSMO solvation model for calculating $TSIs_{asymm}$ (Figures 5 and 6). Results are depicted in Figure 11, where energy profiles for the O-O bond breaking of H_2O_2 in the presence of two acetonitrile molecules, OTf^- and four water molecules are compared to that shown in Figure 5 taken as reference (only COSMO).

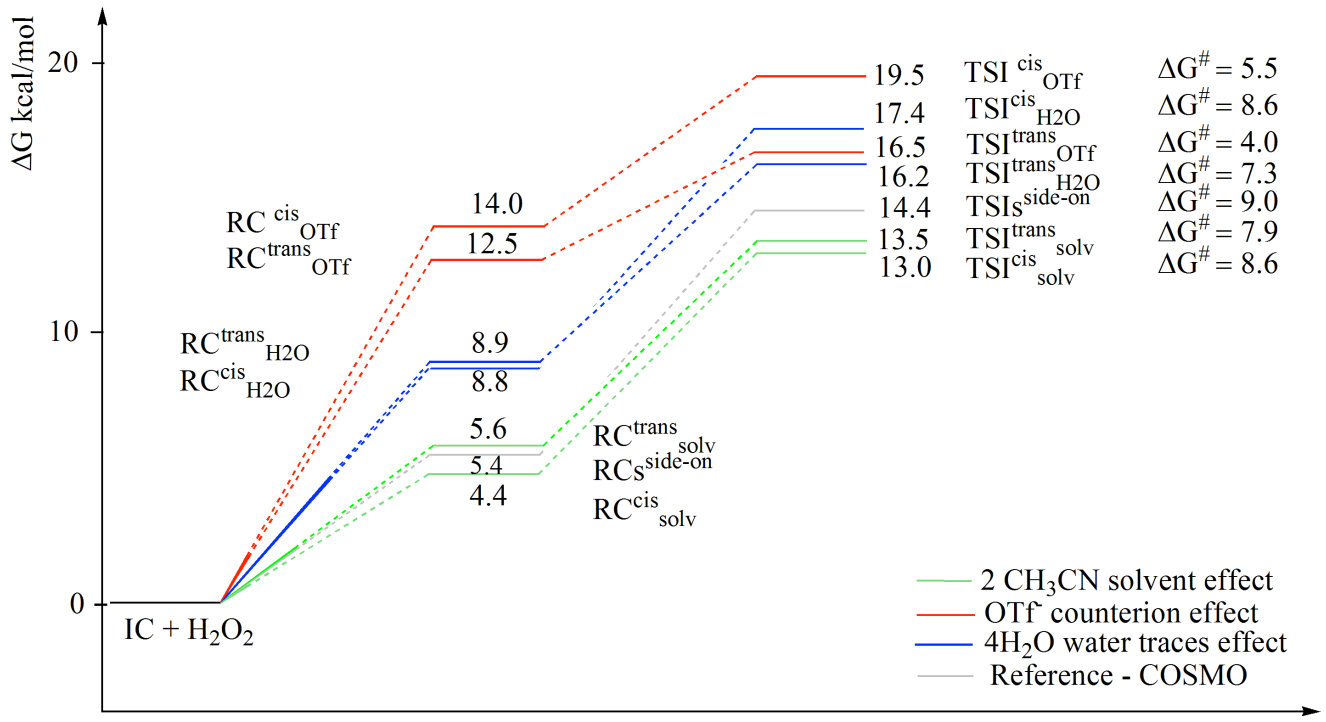

Figure 11. Energy profiles for the O-O bond breaking of H_2O_2 in the first dismutation reaction for the sextet spin state. Green lines are for the presence of two explicit acetonitrile molecules, red lines for the inclusion of OTf⁻, blue lines for the presence of four water molecules, and the grey line for solvent included only by the implicit COSMO model (Figure 5). RC^{cis} and TS^{cis} denote reactant complexes and transition states with the same ligand coordination mode (mmf) as in $RCs^{end\text{-}on}$ in Figure 3; RC^{trans} and TS^{trans} represent reactant complexes and transition states with the same ligand coordination mode (fmf) as in $RCs^{side\text{-}on}$ in Figure 3. The sum of the Gibbs free energies of the separate reactants (IC + H_2O_2) (see corresponding ICs in Figure S15 in the SI) is taken as zero reference energy. $\Delta G^{\#}$ values represent the free energy barriers with respect to the reactant complex.

In each case we calculated the corresponding initial complex IC_{solv}, IC_{OTf} and IC_{H2O}, respectively

(geometries are shown in Figure S15 in the SI) and the Gibbs free energies of the separate reactants IC + H_2O_2 are taken as zero reference energy. We should recall here that in the reactant complex in the sextet spin state two different coordination modes around Mn have been found using only COSMO: in the $RCs^{end\text{-}on}$ mmf structure coordination of H_2O_2 occurs in cis position with respect to the central Py ring of the ligand, whereas in the $RCs^{side\text{-}on}$ fmf structure it takes place trans to it, retaining the initial catalyst coordination mode (see Figure 3). Interestingly, inclusion of additional solvent, triflate or water only leads to H_2O_2 binding in an end-on mode to the metal center, both in the $RCs^{end\text{-}on}$–type and $RCs^{side\text{-}on}$ –type coordination around Mn, in contrast to what was found using only COSMO, where the side-on binding of hydrogen peroxide was even preferred by 4.3 kcal/mol over the end-on mode. To account for the two different structures, in Figure 11 the species RCs and TSs with H_2O_2 coordination in cis position with respect to the central Py ring of the ligand are denoted with superscript *cis*, whereas species with H_2O_2 bonded in trans position with superscript *trans*. In RC^{trans} structures, the two Mn-O bond lengths are 2.252 and 2.895 Å with inclusion of two acetonitrile molecules, 2.283 and 2.698 Å with inclusion of four water molecules and 2.178 and 2.797 Å with inclusion of triflate counterion (see Figure S15 in the SI). This finding suggests that H_2O_2 coordinated in the end-on form represents the actual reactive species also in the $RCs^{side\text{-}on}$–type structure and further corroborates the preference for the asymmetric O-O bond breaking process we found before. Notably, the presence of two explicit acetonitrile molecules significantly stabilizes the $RC^{cis}{}_{solv}$ with respect to the reference COSMO $RCs^{end\text{-}on}$ (by 5.3 kcal/mol, compare $RC^{cis}{}_{solv}$ with $RCs^{end\text{-}on}$ in Figure 3), whereas it only slightly destabilizes the $RC^{trans}{}_{solv}$ with respect to $RCs^{side\text{-}on}$ (by 0.2 kcal/mol, compare $RC^{trans}{}_{solv}$ with $RCs^{side\text{-}on}$ in Figure 11). Inclusion of trace amounts of water destabilizes the $RC^{trans}{}_{H2O}$ with respect to $RCs^{side\text{-}on}$ by 3.5 kcal/mol, with $RC^{cis}{}_{H2O}$ and $RC^{trans}{}_{H2O}$ having the same energy (see Figure 11) . Involvement of OTf^- destabilizes the $RC^{trans}{}_{OTf}$ with respect to $RCs^{side\text{-}on}$ by 7.1 kcal/mol, with $RC^{trans}{}_{OTf}$ being preferred over the $RC^{cis}{}_{OTf}$ by 1.5 kcal/mol. Explicit solvent inclusion also slightly stabilizes both transition states $TSI^{trans}{}_{solv}$ and $TSI^{cis}{}_{solv}$ ($TSIs^{side\text{-}on}$ 14.4 kcal/mol in Figure 11), thus decreasing the free energy barrier with

respect to the reactant complex $\Delta G^{\#}$ (7.9 vs. 9.0 kcal/mol for $TSI^{trans}{}_{solv}$ and $TSIs^{side\text{-}on}$, respectively). As a general trend, the $\Delta G^{\#}$ calculated with TSI^{trans}–type coordination species are lower than those computed with the TSI^{cis} –type coordination species. The $\Delta G^{\#}$ is largely decreased in the presence of the counterion (4.0 and 9.0 kcal/mol for $TSI^{trans}{}_{OTf}$ and $TSIs^{side\text{-}on}$, respectively), although the transition state energy is increased (16.5 vs. 14.4 kcal/mol). Finally, the $\Delta G^{\#}$ is slightly decreased (7.3 vs. 9.0 kcal/mol) and the transition state energy is largely enhanced with inclusion of trace amounts of water (16.2 vs. 14.4 kcal/mol). We conclude that the effect of explicit solvent is crucial in determining the actual reactive species in the first dismutation reaction, which is the H_2O_2 coordinated in the end-on form. Remarkably, inclusion of explicit solvent also stabilizes the end-on coordination mode of H_2O_2 to the metal center in cis position with respect to the central ligand Py ring, which becomes more stable than the H_2O_2 coordination trans to it (4.4 vs. 5.6 kcal/mol, respectively). In addition, inclusion of explicit solvent affects the activation barrier for the O-O bond breaking, which is slightly decreased (7.9 and 8.6 vs. 9.0 kcal/mol, respectively). Both trace amounts of water and OTf` increase the reactant complex and the transition state energy with respect to the separate reactants , which will not favor this process. Finally, since we have found that the activation energy barrier for the RDS of the first dismutation reaction is slightly decreased by inclusion of explicit solvent molecules, we expect that insertion of two explicit acetonitrile molecules will influence the activation energy barrier for the RDS of the second dismutation reaction along the sextet pathway. Optimization calculations performed on II_{OH}s and $TSII_{OH}$s are depicted in Figure S16 in the SI. Similarly, $\Delta G^{\#}$ is found to decrease slightly from 10.5 kcal/mol (COSMO only) to 9.0 kcal/mol. On the basis of these findings, we can reasonably conclude that O-O bond breaking process in the first dismutation reaction can be considered the RDS for the overall reaction for the dihydroxo pathway, whereas both the O-O bond breaking in the first dismutation reaction and the second hydrogen abstraction from H_2O_2 in the second dismutation process have very close activation barriers (7.9 and 9.0 kcal/mol, respectively) for the ping-pong pathway. Molecular dynamic calculations, which are beyond the scope of this paper, would be useful to

definitely discriminate the RDS for the overall reaction between these two steps and to elucidate the role of a viable H_2O_2 coordination in a cis position with respect to the central Py ring of the ligand in the reactant complex in the first dismutation reaction.

4.Conclusions

The present work describes a DFT S12g functional computational study on the mechanism of H_2O_2 dismutation reaction catalyzed by the $[MnS_2Py_3(OTf)_2]$ complex that acts as a catalase mimic and for which experimental data are available.[23] In our calculations the complex has been preventively analyzed in terms of coordination properties since experimental X-ray structural data were lacking. We found that a $[MnS_2Py_3]^{2+}$ complex in a distorted square pyramidal coordination geometry is the proper catalyst for the reaction with the peroxide molecule. The sextet, quartet and doublet potential energy profiles of the catalytic reaction have been explored.

In the first dismutation reaction the rate-determining step is found to be the asymmetric O-O bond cleavage, which occurs on the sextet potential energy profile. A subsequent spin crossover from sextet to quartet, driven by a geometry coordination change at the metal center, can take place generating a stable Mn(IV) dihydroxo intermediate which represents a deactivated form of the catalyst in the ping-pong mechanism. However, we have shown that the formation of this stable intermediate paves the way to an alternative reaction pathway for the second dismutation process, termed the dihydroxo mechanism. These two competing channels have different spin states: the sextet reaction pathway corresponds to a ping-pong mechanism, whereas the quartet reaction follows preferably a dihydroxo mechanism where the two water molecules and dioxygen are very easily and simultaneously formed in the second dismutation process. The reaction mechanism is controlled by a spin state crossover triggered by Mn coordination switching from octahedral (in the

ping-pong route) to trigonal prismatic (in the dihydroxo path). The doublet reaction path is unimportant for both channels since it is always energetically disfavored. Our results suggest that the bottleneck for the whole dismutation process is however the O-O bond breaking step in the first dismutation process for the dihydroxo pathway, whereas both the O-O bond breaking step in the first dismutation process and the second hydrogen abstraction from H_2O_2 in the second dismutation process present very close activation barriers for the ping-pong pathway. Explicit solvent, counterion and traces of water inclusion further supports the preference for the asymmetric O-O bond breaking by favoring the H_2O_2 end-on coordination mode. This finding can be ascribed to the steric effects exerted by these external species on coordination geometries which, due to the absence of any crystal field stabilization energy for the high-spin d^5 Mn complex, are subjected to a facile intramolecular ligand reorganization process. Inclusion of explicit solvent molecules slightly decreases the activation energy barrier, as well as trace of water and counterion involvement, although in the latter cases as a consequence of the destabilization of the corresponding reactant complexes. In addition, explicit solvent calculations suggest the possibility that an alternative coordination site of the first substrate molecule to the metal, namely a reactant complex with H_2O_2 in cis position with respect to the central Py ring of the ligand instead of in trans to it, could also be a reactive species in the dismutation process. Analogously, inclusion of explicit solvent molecules slightly decreases the activation energy barrier for the second hydrogen abstraction from H_2O_2 in the second dismutation reaction. The present study on the mechanism of the catalase-like activity of $[MnS_2Py_3]^{2+}$ complex would benefit from explicit-solvent molecular dynamic simulations, which are however beyond the scope of this paper, that can increase the information to aid in the evaluation of the preferred pathway. It is important to point out that on the basis of our detailed analysis of the mode of action of the $[MnS_2Py_3]^{2+}$- catalase mimic we can confirm the experimental evidence that a monomeric Mn(IV) dihydroxo complex can represent the activated form of the catalyst in some oxidation reactions. Moreover, the current work, disclosing an alternative reaction path for a Mn (II) complex bearing a pentadentate NSNSN ligand, could be helpful for further

improvement in the structural design of manganese complexes as synthetic catalytic scavengers of hydrogen peroxide of pharmaceutical relevance.

Associated content

Supporting Information

Details of the mechanistic computational study, optimized geometries, spin density distribution for all the species and Cartesian coordinates for all the calculated structures.

Author information

Corresponding Authors:

*E-mail for M.S.: marcel.swart@icrea.cat

*E-mail for P.B.: paola.belanzoni@unipg.it

Notes

The authors declare no competing financial interest.

Acknowledgements

This work has been carried out in the framework of the COST action CM1305 “Explicit Control Over Spin-states in Technology and Biochemistry (ECOSTBio)”.

References:

1) Gutteridge, J.M.C.; Halliwell, B. *Free Radical Biol. Med.* **1992**, *12*, 93-94.
2) Halliwell, B. *Lancet* **1994**, *344*, 721-724.
3) Barynin, V.V.; Whittaker, M.M.; Antonyuk, S.V.; Lamzin, V.S.; Harrison, P.M.; Artymiuk,

P.J.; Whittaker, J.W. *Structure* **2001**, *9*, 725-738.

4) Signorella, S.; Hureau, C. *Coord. Chem. Rev.* **2012**, 256, 1229-1245.

5) Wu, A.J.; Penner-Hahn, J.; Pecoraro, V.L. *Chem. Rev.* **2004**, *104*, 903-938.

6) Mathur, P.; Crowder, M.; Dismukes, G.C. *J. Am. Chem. Soc.* **1987**, *109*, 5227-5233.

7) Melov, S.; Ravenscroft, J.; Malik, S.; Gill, M.S.; Walker, D.W.; Clayton, P.E.; Wallace, D.C.; Malfroy, B.; Doctrow, S.R.; Lithgow, G.J. *Science* **2000**, *289*, 1567-1569.

8) Iranzo, O. *Bioorg. Chem.* **2011**, *39*, 73-87.

9) Riley, D.P.; Schall, O.F. *Adv. Inorg. Chem.* **2007**, *59*, 233-263.

10) Giblin, G.M.P.; Box, P.C.; Campbell, I.B.; Hancock, A.P.; Roomans, S.; Mills, G.I.; Molloy, C.; Tranter, G.E.; Walker, A.L.; Doctrow, S.R.; Huffman, K.; Malfroy, B. *Bioorg. Med. Chem. Lett.* **2001**, *11*, 1367-1370.

11) Doctrow, S.R.; Huffman, K.; Marcus, C.B.; Tocco, G.; Malfroy, E.; Adinolfi, C.A.; Kruk, H.; Baker, K.; Lazarowych, N.; Mascarenhas, J.; Malfroy, B. *J. Med. Chem.* **2002**, *45*, 4549-4558.

12) Salvemini, D.; Wang, Z.-Q.; Zweier, L.; Samouilov, A.; Macarthur, H.; Misko, T.P.; Currie, M-G-; Cuzzocrea, S.; Sikorski, J.A.; Riley, D.P. *Science* **1999**, *286*, 304-306.

13) Singh, O.; Tyagi, N.; Olmstead, M.M.; Ghosh, K. *Dalton Trans.* **2017**, *46*, 14186-14191.

14) Palopoli, C.; Gómez, G.; Foi, A.; Doctorovich, F.; Mallet-Ladeira, S.; Hureau, C.; Signorella, S. *J. Inorg. Biochem.* **2017**, *167*, 49-59.

15) Squarcina, A.; Soraru, A.; Rigodanza, F.; Carraro, M.; Brancatelli, G.; Carofiglio, T.; Geremia, S.; Larosa, V.; Morosinotto, T.; Bonchio, M. *ACS Catal.* **2017**, *7*, 1971-1976.

16) Ledesma, G. N.; Eury, H.; Anxolabehere-Mallart, E.; Hureau, C.; Signorella, S. *J. Inorg. Biochem.* **2015**, *146*, 69-76.

17) Noritake, Y.; Umezawa, N.; Kato, N.; Higuchi, T. *Inorg. Chem.* **2013**, *52*, 3653-3662.

18) Kovacs, J. *Acc. Chem. Res.* **2015**, *48*, 2744-2753.

19) Brazzolotto, D.; Reinhard, F.G.C.; Smith-Jones, J.; Retegan, M.; Amidani, L.; Faponle, A.S.; Ray, K.; Philouze, C.; de Visser, S.P.; Gennari, M.; Duboc, C. *Angew. Chem. Int. Ed.* **2017**, *56*, 8211-8215.

20) Yosca, T.H.; Ledray, A.P.; Ngo, J.; Green, M.T. *J. Biol. Inorg. Chem.* **2017**, *22*, 209-220.

21) Gennari, M.; Brazzolotto, D.; Pecaut, J.; Cherrier, M.V.; Pollock, C.J.; DeBeer, S.; Retegan, M.; Pantazis, D.A.; Neese, F.; Rouzieres, M.; Clerac, R.; Duboc, C. *J. Am. Chem. Soc.* **2015**, *137*, 8644-8653.

22) McQuilken, A.C.; Goldberg, D.P. *DaltonTrans.* **2012**, *41*, 10883-10899.

23) Grau, M.; Rigodanza, F.; White, A.J.P.; Sorarù, A.; Carraro, M.; Bonchio, M.; Britovsek, G.J.P. *Chem. Commun.* **2014**, *50*, 4607-4609.

24) Widger, L.R.; Jiang, Y.B.; McQuilken, A.C.; Yang, T.S.; Siegler, M.A.; Matsumura, H.; Moenne-Loccoz, P.; Kumar, D.; de Visser, S.P.; Goldberg, D.P. *Dalton Trans.* **2014**, *43*, 7522-7532.

25) Herdt, D.R.; Grapperhaus, C.A. *Dalton Trans.* **2012**, *41*, 364-366.

26) Dürr, K.; Yalalov, D.A.; Heinemann, F.W.; Tsogoeva, S.B.; Ivanovic-Burmazovic, I. *Z. Naturforsch* **2010**, *65b*, 258-262.

27) Abashkin, Y.G.; Burt, S.K. *J. Phys. Chem. B* **2004**, *108*, 2708-2711.

28) Abashkin, Y.G.; Burt, S.K. *Inorg. Chem.* **2005**, *44*, 1425-1432.

29) Abashkin, Y.G.; Collins, J.R.; Burt, S.K. *Inorg. Chem.* **2001**, *40*, 4040-4048.

30) Liu, S.-Y.; Soper, J.D.; Yang, J.Y.; Rybak-Akimova, E.V.; Nocera, D.G. *Inorg. Chem.* **2006**, *45*, 7572-7574.

31) Costas, M.; Harvey, J.N. *Nat. Chem.* **2013**, *5*, 7-9.

32) Cramer, C.J.; Truhlar, D.G. *Phys. Chem. Chem. Phys.* **2009**, *11*, 10757-10816.

33) Swart, M. *Chem. Phys. Lett.* **2013**, *580*, 166-171.

34) Gruden, M.; Stepanović, S.; Swart, M. *J. Serb. Chem. Soc.* **2015**, *80*, 1399-1410.

35) Daul, C.; Zlatar, M.; Gruden-Pavlović, M.; Swart, M. In *Spin States in Biochemistry and Inorganic Chemistry: Influence on Structure and Reactivity;* Swart, M., Costas, M., Eds;

John Wiley & Sons, Ltd, Oxford, UK, 2015; pp 7-34.

36) Fonseca Guerra, C.; Snijders, J.G.; te Velde, G.; Baerends, E.J. *Theor. Chem. Acc.* **1998**, *99*, 391-403.

37) te Velde, G.; Bickelhaupt, F.M.; Baerends, E.J.; Fonseca Guerra, C.; van Gisbergen, S.J.A.; Snijders, J.G.; Ziegler, T. *J. Comput. Chem*. **2001**, *22*, 931-967.

38) ADF2014.05, SCM, Theoretical Chemistry, Vrije Universiteit, Amsterdam, The Netherlands, http://www.scm.com

39) Swart, M.; Bickelhaupt, F.M. *J. Comput. Chem.* **2008**, *29*, 724-734.

40) Becke, A.D. *Phys. Rev. A* **1988**, *38*, 3098-3100.

41) Perdew, J.P. *Phys. Rev. B* **1986**, *33*, 8822-8824

42) Grimme, S.; Ehrlich, A.J.; Goerigk, L. *J. Comput. Chem.* **2011**, *32*, 1456-1465.

43) Klamt, A.; Schüürmann, G. *J. Chem. Soc.: Perkin Trans.* **1993**, *2*, 799-805.

44) Klamt, A. *J. Phys. Chem.* **1995**, *99*, 2224-2235.

45) Klamt, A.; Jones, V. *J. Chem. Phys.* **1996**, *105*, 9972-9981.

46) van Lenthe, E.; Baerends, E.J.; Snijders, J.G. *J. Chem. Phys.* **1994**, *101*, 9783-9792.

47) van Lenthe, E.; van Leeuwen, R.; Baerends, E.J.; Snijders, J.G. *Int. J. Quantum Chem.* **1996**, *57*, 281-293.

48) Swart, M.; Gruden, M. *Acc. Chem. Res.* **2016**, *49*, 2690-2697.

49) Swart, M.; Solà, M.; Bickelhaupt, F.M. *J. Comp. Meth. Sci. Engin.* **2009**, *9*, 69-77.

50) Swart, M. *J. Chem. Theory Comput.* **2008**, *4*, 2057-2066.

51) Swart, M.; Solà, M.; Bickelhaupt, F.M. *J. Chem. Phys.* **2009**, *131*, 094103.

52) Grimme, S. *J. Comput. Chem.* **2006**, *27*, 1787-1799.

53) Grimme, S.; Ehrlich, A.J.; Krieg, H. *J. Chem. Phys.* **2010**, *132*, 154104.

54) Padamati, S.K; Angelone, D.; Draksharapu, A.; Primi, G.; Martin, D.J.; Tromp, M.; Swart, M.; Browne, W.R. *J. Am. Chem. Soc.* **2017**, *139*, 8718-8724.

55) Grau, M.; England, J.; Torres Martin de Rosales, R.; Rzepa, S.; White, A.J.P.; Britovsek,

G.J.P. *Inorg. Chem.* **2013**, *52*, 11867-11874.

56) Swart, M.; van Duijnen, P. T.; Snijders, J.G. J. *J. Comput. Chem.* **2001**, *22*, 79-88.

57) Carra, B.J.; Till, S.N.; VanGundy, R.A.; Pike, R.D.; Bebout, D.C. Polyhedron **2016**, *114*, 278-285.

58) Sproules, S.; Wieghardt, K. *Coord. Chem. Rev.* **2011**, *255*, 837-860

59) Wang, Y.; Shi, S.; Zhu, D.; Yin, G. *Dalton Trans.* **2012**, *41*, 2612-2619.

60) Kurahashi, T.; Kikuchi, A.; Shiro, Y.; Hada, M.; Fujii, H. *Inorg. Chem.* **2010**, *49*, 6664-6672.

61) Xu, A.; Xiong, H.; Yin, G. *Chem. Eur. J.* **2009**, *15*, 11478-11481.

62) Yin, G. Danby, A.M.; Kitko, D.; Carter, J.D.; Scheper, W.M.; Busch, D.H. *J. Am. Chem. Soc.* **2008**, *130*, 16245-16253.

63) Yin, G.; Danby, A.M.; Kitko, D.; Carter, J.D.; Scheper, W.M.; Busch, D.H. *J. Am. Chem. Soc.* **2007**, *129*, 1512-1513.

64) Drzewiecka-Matuszek, A.; Rutkowska-Zbik, D.; Witko, M. *Can. J. Chem.* **2013**, *91*, 642-647.

65) Mallick, D.; Shaik, S. *ACS Catal.* **2016**, *6*, 2877-2888.

66) Goldstein, S.; Meyerstein, D.; Czapski, G. *Free Radic. Biol. Med.* **1993**, *15*, 435-445.

67) Khavrutskii, I.V.; Rahim, R.R.; Musaev, D.G; Morokuma, K. *J. Phys. Chem. B* **2004**, *108*, 3845-3854.

68) Lansky, D.E.; Narducci Sarjeant, A.A.; Goldberg, D.P. *Angew. Chem. Int. Ed.* **2006**, *45*, 8214-8217.

69) Annaraj, J.; Cho, J.; Lee, Y.-M.; Kim, S.Y.; Latifi, R.; de Visser, S.P.; Nam, W. *Angew. Chem. Int. Ed.* **2009**, *48*, 4150-4153.

70) Yin, G.; McCormick, J.M.; Buchalova, M.; Danby, A.M.; Rodgers, K.; Day, V.W.; Smith, K.; Perkins, C.M.; Kitko, D.; Carter, J.D.; Scheper, W.M.; Busch, D.H. *Inorg. Chem.* **2006**, *45*, 8052-8061.

71) Garcia-Bosch, I.; Company, A.; Cady, C.W.; Styring, S.; Browne, W.R.; Ribas, X.; Costas, M. *Angew. Chem. Int. Ed.* **2011**, *50*, 5648-5653.

72) Lee, W.-T.; Xu, S.; Dickie, D.A.; Smith, J.M. *Eur. J. Inorg. Chem.* **2013**, 3867-3873.

73) Michel, C.; Baerends, E.J. *Inorg. Chem*. **2009**,*48*, 3628-3638.

74) Meunier, B.; de Visser, S.P.; Shaik, S. *Chem. Rev*. **2004**, *104*, 3947-3980.

75) Gopakumar, G.; Belanzoni, P.; Baerends, E.J. *Inorg. Chem*. **2012**, *51*, 63-75.

76) Chen, J.; Cho, K.-B.; Lee, Y.-M.;Kwon, Y.H.; Nam, W. *Chem. Commun.* **2015**, *51*, 13094-13097.

77) Cho, K.-B.; Shaik, S.; Nam, W. *J. Phys. Chem. Lett.* **2012**, *3*, 2851-2856.

78) Leto, D.F.; Massie, A.A.; Rice, D.B.; Jackson, T.A. *J. Am. Chem. Soc.* **2016**, *138*, 15413-15424.

79) Hull, J.F.; Balcells, D.; Sauer, E.L.O.; Raynaud, C.; Brudvig, G.W.; Crabtree, R.H.; Eisenstein, O. *J. Am. Chem. Soc.* **2010**, *132*, 7605-7616.

Graphical Abstract